

# Inf-suf stable bES-FEM method for nearly incompressible elasticity

Thanh Hai Ong<sup>1,4</sup>, G. R. Liu<sup>2</sup>, T. Nguyen-Thoi<sup>3,4</sup>, H. Nguyen-Xuan<sup>3,4</sup>

<sup>1</sup>*Department of Analysis, Faculty of Mathematics Computer Science, University of Science, VNU-HCMC, Nguyen Van Cu Street, District 5, Ho Chi Minh City 700000, Viet Nam.*

<sup>2</sup>*School of Aerospace Systems, University of Cincinnati, 2851 Woodside Dr, Cincinnati, OH 45221, USA.*

<sup>3</sup>*Department of Mechanics, Faculty of Mathematics Computer Science, University of Science, VNU-HCMC, Nguyen Van Cu Street, District 5, Ho Chi Minh City 700000, Viet Nam.*

<sup>4</sup>*Division of Computational Mechanics, Ton Duc Thang University, Nguyen Huu Tho Street, District 7, Ho Chi Minh City 700000, Viet Nam.*

May 21, 2013

## Abstract

This paper introduces the improved edge-based smoothed finite element method (bES-FEM) on simplices to solve the nearly incompressible elasticity problem. The improved method uses the piecewise linear polynomial space enriched with a bubble function on each element for the displacement, and the discontinuous pressure which is defined on a third mesh satisfies the uniform inf-suf condition. Moreover, the bES-FEM method induces a further softening to the bilinear form allowing the weakened weak (W2) procedure to get a quality solution. Several numerical examples are provided to show the effectiveness and reliability of the bES-FEM method.

## 1 Introduction

Elasticity materials such as rubber and rubber-like materials are used so much in the industry, we then have to research their structure and resort to approximate structural-analysis techniques. One of important features in the stress analysis of these materials is the nearly-incompressible case, i.e their bulk moduli are much

larger than their shear moduli, or the Poisson ratio is near to one half. Computationally, if we apply low-order finite elements based on quadrilaterals, hexahedra or simplices to solve a nearly incompressible elasticity problems, these methods are well-known to be the locking-effect. Until now, there are several numerical methods suggested to overcome this poor phenomena, for examples: the h-version finite elements [3, 4] result in poor observed convergence rates in the displacement, the B-bar method [15] for linear and nonlinear elasticity is leaded from separation of volumetric and deviatoric, the mixed formulations [1, 7, 8] having the independent displacement and pressure fields, enhanced assumed strain (EAS) modes [39, 40, 41], reduced integration stabilization [42]-[46], two-field mixed stress elements [47]. Besides, we have several publications focusing on the analysis of average nodal pressure formulation based on enforcing a constant pressure field over a patch of triangles or tetrahedra [48, 49, 50, 51, 26]. It is easy to implement such scheme in the existing codes and has many nice properties. Although there exist many approaches to solve a nearly incompressible elasticity problem on the triangulation, a few methods are based on the rigorous mathematical analysis. For example [26], the author introduced the method whose the pressure is discontinuous, and the displacement space belongs to the piecewise linear polynomial space of FEM enriched with a bubble function per element for the displacement. This method is based on the rigorous mathematical analysis. However, this displacement space certain has drawbacks of the FEM method: 1) overestimation of stiffness matrix especially for nearly incompressible and bending dominated problems, 2) poor performances when meshes are distorted, 3) poor accuracy for stresses.

In this paper, we propose a new finite element method called by the edge-based smooth finite element method enriched by bubble functions (bES-FEM) for nearly incompressible elasticity problems, where the usual two types consisting of the  $\xi$ th-power bubble functions with  $\xi = 3(2D), 4(3D)$  and the hat bubble functions are used. The bES-FEM method is designed in order to inherit advantages of some classical methods. Firstly, we use mixed methods [1, 5] to reformulate from the linear elasticity problem (1) into the mixed displacement-pressure problem (5), which leads to yield good approximations to the pressure as well [3]. The pressure is piecewise constants on the third mesh, the degree of freedom associating with the pressure variable can be computed by linear combinations depending on the displacement variable. Secondly, the approximation displacement is combined by the edge-based smooth finite element method (ES-FEM) [23] and the bubble functions [28], [25]. The ES-FEM method is a member of the smooth finite element S-FEM family including the cell-based smoothed finite element method (CS-FEM) [21], the node-based smooth finite element method (NS-FEM) [22], the edge-based smooth finite element method (ES-FEM) and the face-based smooth finite element (FS-FEM) [24]. Moreover, in [9], the authors investigated the extension of the ES-FEM method to 3D. The essential idea in the S-FEM family is to reconstruct the compatible strain field in finite element settings using the strain smoothing technique [12]. The reconstructed strain field is obtained over various sub-domains called smoothing domains created on cells (CS-FEM), nodes (NS-FEM), edges (ES-FEM) or faces (FS-FEM) of the mesh background, and the art

of the S-FEM family is the innovative design of the smoothing domains for desired amount of softening effects. The numerical operations used in the S-FEM family bring in information from the neighboring elements in desired ways. Depends on the requirements of the analyst, the property of an S-FEM model can be distinct in various ways from that of the standard FEM model. The S-FEM family can also be viewed as a combination of the numerical treatments of both used in the FEM and meshfree methods [19]. Since smoothing domains in the S-FEM family often (not always) cover part of the adjacent elements, the number of supporting nodes associated with the smoothing domain is larger than the number of nodes of an element. As a result, the bandwidth of the stiffness matrix (if formed) in the S-FEM family is increased, and the computational cost is hence higher than the standard FEM with the same sets of nodes. On the other hand, thanks to the propagation of non-local information brought by the adjacent elements, the S-FEM family often produces much more accurate solutions than the standard FEM method. For a given computational cost, all S-FEM models have better accuracy than that of the displacement-based FEM [15, 29]. The S-FEM models were applied to a wide range of practical mechanics problems [30]-[37], and the S-FEM family has become a simple and effective tool for the analysis of a variety of practical problems. Among the existing S-FEM models, the ES-FEM was found so far the most computationally efficient [20]. Hence, the ES-FEM exhibits some interesting properties for solid mechanics problems such as: 1) it produces much more accurate solutions than the linear triangular elements (FEM-T3) and often found even more accurate than the FEM using quadrilateral elements (FEM-Q4) using the same sets of nodes; 2) the ES-FEM performs well with distorted meshes; 3) it is super-accurate and has super-convergent properties in stress solutions; 4) the ES-FEM is stable even for dynamic analysis and 5) it is simple to implement into the existing FEM packages without any additional degrees of freedom. However, if the displacement is only approximated by the ES-FEM method without enriching the bubbles functions, this method also is violated the in-suf condition, which is proved in this paper. Thirdly, using the bES-FEM method, we show that the inf-suf condition satisfies uniformly for the discontinuous pressure defined on a third mesh. The degree of freedom associating with the pressure variable can be computed by linear combinations depending on the displacement variable, which is a important feature be different from the classical mini element [5].

The organization of the rest of this paper is outlined as follows. In the next section, we briefly recall the boundary-value of linear elasticity problems, the mixed displacement-pressure form and weak form. Section 3 represents the description of ES-FEM method with bubble enrichment. Section 4 shows the mathematical properties of the bES-FEM method. Displacement, energy and pressure error norms are defined in Section 5 for precise qualitative examination of various models. Several numerical examples are presented in section 6. Section 7 concludes with some main remarks and discussions on directions for future work.

## 2 The boundary-value of linear elasticity

We consider a static linear elasticity problem governed by equilibrium equations in a bounded domain  $\Omega \subset \mathbb{R}^d$ ,  $d = \{2, 3\}$  with the Lipschitz boundary  $\partial\Omega$ .

$$- \operatorname{div} \sigma = f \quad \text{in } \Omega. \quad (1)$$

Displacements  $u$  are prescribed on the boundary  $\partial\Omega$

$$u = 0 \quad \text{on } \Gamma. \quad (2)$$

In the elasticity problem, the relations between the displacement field  $u$ , the strain field  $\varepsilon$  and the stress field  $\sigma$  are:

- The compatibility relation between the strains and displacements

$$\forall i, j = \overline{1, d} : \varepsilon_{ij}(u) = \frac{1}{2} (\partial_j u_i + \partial_i u_j) \quad \text{in } \Omega, \quad (3)$$

where  $\partial_i = \frac{\partial}{\partial x_i}$  with  $(x_1, \dots, x_d) \in \mathbb{R}^d$ ,  $\varepsilon(u) = [\varepsilon_{ij}(u)]_{i,j=\overline{1,d}}$ .

- The constitutive relations for elastic solids can be given as

$$\sigma_{ij}(u) = \lambda \delta_{ij} \varepsilon_{kk}(u) + 2\mu \varepsilon_{ij}(u) \quad \text{in } \Omega \quad \text{or} \quad \sigma(u) = D\varepsilon(u) \quad \text{in } \Omega, \quad (4)$$

where  $\mu = \frac{E}{2(1+\nu)}$ ,  $\lambda = \frac{\nu E}{(1+\nu)(1-2\nu)}$  are the Lamé constants and  $\delta_{ij}$  is the Kronecker delta index and  $D$  is the Hooke elastic matrix.

Our attention is devoted to the nearly incompressible case which corresponds to  $\nu$  being very near to 0.5. This case leads to the poor performance that is well known to be the locking effect and instability.

### 2.1 Mixed displacement-pressure form and weak form

The elasticity problem (1) can be rewritten by the following mixed displacement-pressure form

$$- \operatorname{div} \sigma = f \quad \text{in } \Omega, \quad (5)$$

$$\operatorname{div} u - \frac{p}{\lambda} = 0 \quad \text{in } \Omega, \quad (6)$$

where a pressure  $p$  is introduced as a extra variable. The mixed form is the same as penalized Stokes equations.

The mixed approach finds a displacement field  $u \in V = [\mathbb{H}^1(\Omega)]^d$  and a pressure  $p \in L_0^2(\Omega) := \left\{ q \in L^2(\Omega) : \int_{\Omega} q \, dx = 0 \right\}$  that satisfy

$$a(u, v) + b(v, p) = (f, v) \quad \forall v \in V_0, \quad (7)$$

$$b(q, u) - \frac{1}{\lambda} c(p, q) = 0 \quad \forall q \in L_0^2(\Omega), \quad (8)$$

where  $p$  belongs to  $L_0^2(\Omega)$  because of the Dirichlet boundary condition, and the bilinear forms are defined, as follows:

$$\begin{aligned} a(u, v) &= 2\mu \int_{\Omega} \varepsilon^T(u(x)) D \varepsilon(v(x)) \, dx, \\ b(q, u) &= \int_{\Omega} q(x) \nabla \cdot u(x) \, dx, \\ c(q, p) &= \int_{\Omega} q(x) p(x) \, dx, \\ (f, v) &= \int_{\Omega} f(x) v(x) \, dx, \end{aligned}$$

with  $f \in L^2(\Omega)$ , the matrix  $D$  of material constants is symmetric, positive definite and its eigenvalues are bounded in  $[a, b] \subset \mathbb{R}^+$ .

### 3 Description of ES-FEM method with bubble enrichment

#### 3.1 The meshes and the finite spaces

The polygon domain  $\Omega$  is discretized by the triangulation  $\mathcal{T}_h$  (the primal mesh), where  $\mathcal{T}_h$  consists of simplices, either triangles or tetrahedra. The set  $\mathcal{T}_h$  has  $N_e$  elements,  $N_n$  nodes (or vertices),  $N_s$  edges and  $\overline{\Omega} = \bigcup_{i=1, T_i \in \mathcal{T}_h}^{N_e} \overline{T_i}$ . For each element  $T \in \mathcal{T}_h$ , the barycentric point  $c_T$  is called a mesh point of  $T$ . Let  $\mathcal{V}_h$  be the standard linear finite element space defined on the triangulation  $\mathcal{T}_h$ ,

$$\mathcal{V}_h = \left\{ u \in [H^1(\Omega)]^d, \, u|_T \in [\mathcal{P}^1(\Omega)]^d \right\}$$

which has the standard nodal basic functions  $N_i$  ( $i = \overline{1, N_n}$ ) associated with the node  $i$ .

Defining the space of bubble functions as

$$\mathcal{B}_h = \left\{ b_T \in H^1(\Omega), \, b_T|_{\partial T} = 0 \text{ and } \int_T b_T(x) dx > 0, T \in \mathcal{T}_h \right\},$$

where the basis bubble functions are considered in two types (see [28] and [25]), on each element  $T \in \mathcal{T}_h$ ,

- The first one is the  $\xi$ th-power bubble function with  $\xi = d + 1$

$$b_T(x) = \begin{cases} c_b(d+1)^3 \prod_{i=1}^{d+1} \lambda_{T(i)}(x), & \text{if } x \in T \subset \mathcal{T}_h, \\ 0 & \text{elsewhere} \end{cases} \quad (9)$$

where each function  $\lambda_{T(i)}$  is a barycentric coordinate associated with a vertex  $x_{T(i)}$  of the triangle  $T$ , and  $c_b$  is computed in such a way that  $b_T(c_T) = 1$  with the centroid  $c_T$  of  $T$ .

- The second one is the hat function on  $T$ , where  $T$  is partitioned into sub-triangles (2D) or sub-tetrahedra (3D)  $\{T_{(i)}\}_{i=\overline{1,d+1}}$  by joining the centroid  $c_T$  to the two vertices (2D) or the three vertices (3D)

$$b_T(x) = \begin{cases} c_b(d+1)\lambda_{T_{(i)}}(x), & \text{if } x \in T_{(i)} \subset T \subset \mathbb{R}^d, \\ 0 & \text{elsewhere} \end{cases} \quad (10)$$

Using the bubble space  $\mathcal{B}_h$ , the finite element space for the displacement which is enriched with bubble functions is defined as  $\mathcal{V}_h^{\mathcal{B}} = \mathcal{V}_h \oplus [\mathcal{B}_h]^d \subset [\mathbb{H}^1(\Omega)]^d$ . Each function  $u_h \in \mathcal{V}_h^{\mathcal{B}}$  which is restricted on  $T \in \mathcal{T}_h$  is written as

$$u_h(x) = \underbrace{\sum_{i=1}^{d+1} \text{diag} \left( \underbrace{N_{T_{(i)}}(x), \dots, N_{T_{(i)}}(x)}_{d \text{ dimensions}} \right) u_{T_{(i)}}}_{\ell_h(x) \in \mathcal{V}_h} + \underbrace{\text{diag} \left( \underbrace{N_{c_T}^b(x), \dots, N_{c_T}^b(x)}_{d \text{ dimensions}} \right) u_{c_T}}_{b_h(x) \in [\mathcal{B}_h]^d}, \quad (11)$$

where the diagonal matrix is denoted by  $\text{diag}(\cdot)$ , for each  $i = \overline{1, d+1}$ ,  $N_{T_{(i)}}$  is the standard nodal basic function associated with the vertex  $x_{T_{(i)}}$  of the triangle  $T$ ,  $N_{c_T}^b$  is the standard nodal basic cubic bubble function defined on  $T$  with the centroid  $c_T$ . Besides, the values  $u_{T_{(i)}}$  and  $u_{c_T} \in \mathbb{R}^d$  are the nodal values of  $u_h$  at the vertex  $x_{T_{(i)}}$  and the barycenter  $c_T$ .

Furthermore, in order to design a smoothed mesh for smoothing strain and divergence operators, this smoothed mesh that is called a dual mesh  $\mathcal{T}_h^*$  is constructed by connecting all vertices and mesh points of  $\mathcal{T}_h$ . The dual mesh  $\mathcal{T}_h^*$  satisfies  $\overline{\Omega} = \bigcup_{k=1, \Omega_k^s \in \mathcal{T}_h^*}^{N_s} \overline{\Omega}_k^s$ , and all elements of  $\mathcal{T}_h^*$  are not overlapping together. Each element  $\Omega_k^s \in \mathcal{T}_h^*$  is associated with an edge  $e_k$  of the primal mesh  $\mathcal{T}_h$ . For examples, we have an illustration of an element  $\Omega_k^s$  corresponding to an inner edge  $e_k$

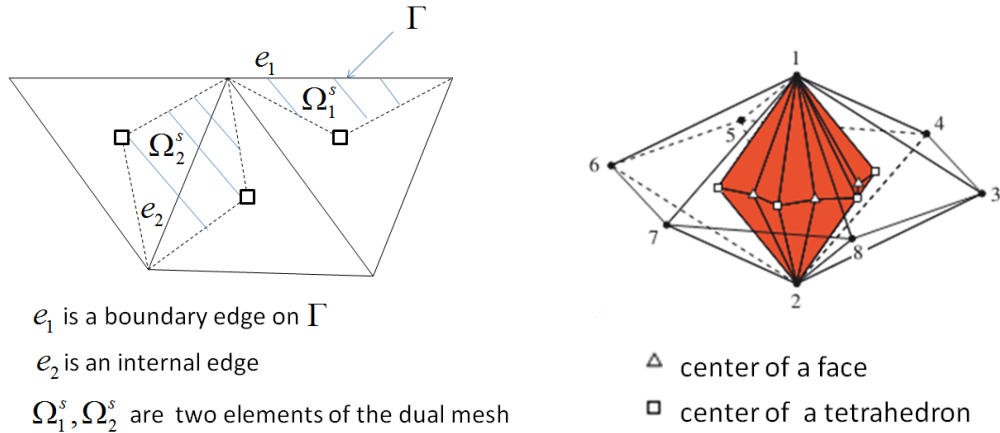


Figure 1

and another illustration of an element  $\Omega_k^s$  located at the boundary

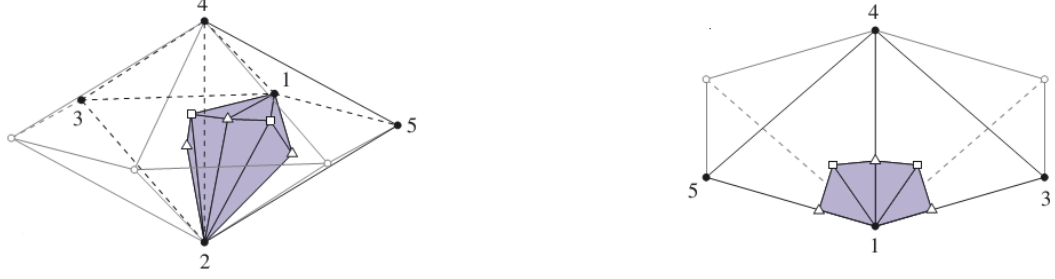


Figure 2

With the dual mesh  $\mathcal{T}_h^*$ , the space  $\mathcal{V}_h^{\mathcal{B}}$  is equipped with the following the inner product, semi-norm and norm (see [17]):

$$\begin{aligned}
(w, v)_{\mathcal{V}_h^{\mathcal{B}}} &= \int_{\Omega} \left( \sum_{i=1}^d w_i v_i \right) dx \\
&+ \sum_{k=1}^{N_s} \text{meas}(\Omega_k^s) \left[ \sum_{i=1}^d \bar{g}_{ii}(w_i) \bar{g}_{ii}(v_i) + \sum_{i=1}^{d-1} \sum_{j=i+1}^d (\bar{g}_{ij}(w_i) + \bar{g}_{ji}(w_j)) (\bar{g}_{ij}(v_i) + \bar{g}_{ji}(v_j)) \right] \\
|w|_{\mathcal{V}_h^{\mathcal{B}}} &= \sum_{k=1}^{N_s} \text{meas}(\Omega_k^s) \left[ \sum_{i=1}^d \bar{g}_{ii}^2(w_i) + \sum_{i=1}^{d-1} \sum_{j=i+1}^d (\bar{g}_{ij}(w_i) + \bar{g}_{ji}(w_j))^2 \right], \\
\|w\|_{\mathcal{V}_h^{\mathcal{B}}} &= \int_{\Omega} \left( \sum_{i=1}^d w_i^2 \right) dx + \sum_{k=1}^{N_s} \text{meas}(\Omega_k^s) \left[ \sum_{i=1}^d \bar{g}_{ii}^2(w_i) + \sum_{i=1}^{d-1} \sum_{j=i+1}^d (\bar{g}_{ij}(w_i) + \bar{g}_{ji}(w_j))^2 \right],
\end{aligned}$$

where vectors  $w = (w_1, \dots, w_d), v = (v_1, \dots, v_d)$  belong to  $\mathcal{V}_h^{\mathcal{B}}$ ,  $\bar{g}_{ij}(w_i) = \overline{\frac{\partial w_i}{\partial x_j}} = \frac{1}{\text{meas}(\Omega_k^s)} \int_{\Omega_k^s} \frac{\partial w_i}{\partial x_j}(x) dx$  on a smooth element  $\Omega_k^s \in \mathcal{T}_h^*$ , and the measure  $\text{meas}(\Omega_k^s)$  is equal to  $\int_{\Omega_k^s} 1 dx$ .

Thank to the remarks 3.4 and 3.5 of [17], we have relationships between  $|\cdot|_{\mathcal{V}_h^{\mathcal{B}}}$ ,  $\|\cdot\|_{\mathcal{V}_h^{\mathcal{B}}}$  and  $|\cdot|_1$ ,  $\|\cdot\|_1$ , as follows:

$$|w|_{\mathcal{V}_h^{\mathcal{B}}} \leq |w|_1 \quad \text{and} \quad \|w\|_{\mathcal{V}_h^{\mathcal{B}}} \leq \|w\|_1 \quad \text{with } w \in \mathcal{V}_h^{\mathcal{B}} \subset H^1(\Omega), \quad (12)$$

where  $H^1(\Omega)$  which is a Sobolev space has the semi-norm  $|\cdot|_1$  and the norm  $\|\cdot\|_1$  defined from the inner product  $(w, v)_1 = \sum_{i=1}^d (w_i, v_i)_1$  (see chapter 3 in [27]).

Next, a third mesh  $\mathcal{T}_h^{**}$  is constructed by connecting all barycentric points  $\{c_T\}_{T \in \mathcal{T}_h}$  and midpoints of all edges of  $\mathcal{T}_h$  in 2D, plus barycentric points of all faces in 3D. The third mesh  $\mathcal{T}_h^{**}$  satisfies  $\bar{\Omega} = \bigcup_{i=1}^{N_n} \bar{V}_i$ , and all elements of

$\mathcal{T}_h^*$  are not overlapping together. Each element  $V_k \in \mathcal{T}_h^{**}$  is also associated with a vertex  $x_k$  of the primal mesh.

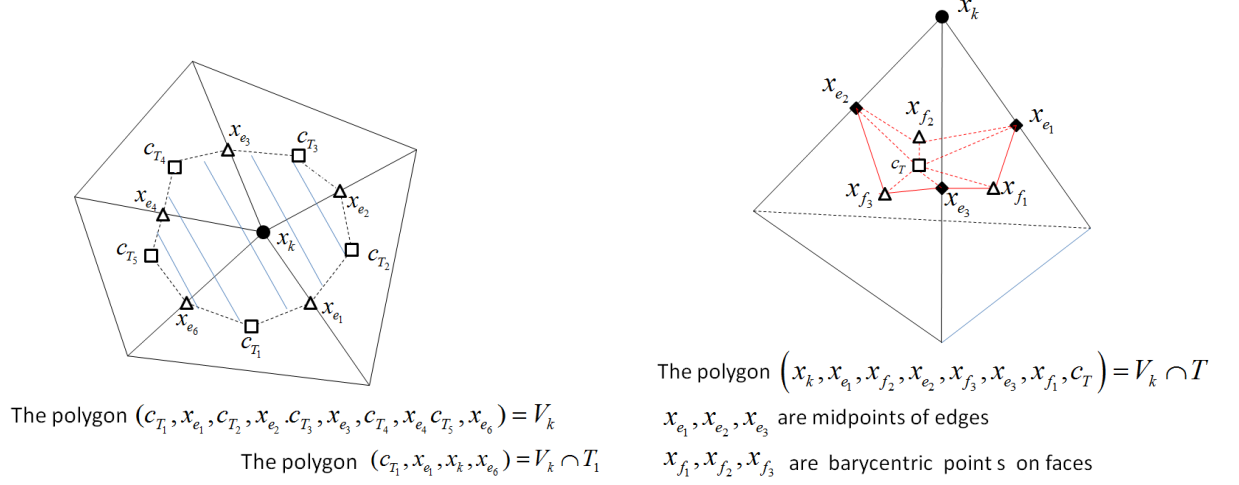


Figure 3

Basing on this third mesh, we define the following finite element space for the pressure

$$\mathcal{V}_h^{**} = \{p \in L_0^2(\Omega) \text{ such that } p|_V \in \mathcal{P}^0(V), V \in \mathcal{T}_h^{**}\},$$

if  $p_h \in \mathcal{V}_h^{**}$ , the function  $p_h = \sum_{i=1}^{N_n} p_i \chi_i$ , where  $\chi_i$  are the characteristic functions of

$V_i \in \mathcal{T}_h^{**}$ ,  $i = \overline{1, N_n}$ , and the norm  $\|\cdot\|_0$  of  $\mathcal{V}_h^{**}$  is defined  $\|q\|_0 = \left(\int_{\Omega} q^2 dx\right)^{\frac{1}{2}}$  with  $q \in \mathcal{V}_h^{**}$ . Now, we represent the bES-FEM method for the nearly incompressible elasticity problem:

### 3.2 Smooth strain and smooth divergence

On each smooth element  $\Omega_k^s \in \mathcal{T}_h^*$ , the strain  $\varepsilon(u_h)$  is smoothed as

$$\bar{\varepsilon}^{(k)}(u_h) = \frac{1}{\text{meas}(\Omega_k^s)} \int_{\Omega_k^s} \varepsilon(u_h)(x) dx \quad \text{with } u_h \in \mathcal{V}_h^{\mathcal{B}}, \quad (13)$$

and for the smoothed divergence, one has

$$(\overline{\nabla \cdot u_h})|_{\Omega_k^s} = \frac{1}{\text{meas}(\Omega_k^s)} \int_{\Omega_k^s} \nabla \cdot u_h(x) dx \quad \text{with } u_h \in \mathcal{V}_h^{\mathcal{B}}. \quad (14)$$

### 3.3 Weakened weak statement for the bES-FEM

Here, we want to find the discrete solution  $(u_h, p_h) \in \mathcal{V}_h^{\mathcal{B}} \times \mathcal{V}_h^{**}$  such that

$$\begin{cases} \bar{a}(u_h, v_h) + \bar{b}(v_h, p_h) = (f, v_h) & \text{with } \forall v_h \in \mathcal{V}_h^{\mathcal{B}}, & (a) \\ \bar{b}(v_h, p_h) - \frac{1}{\lambda} \bar{c}(p_h, q_h) = 0 & \text{with } \forall q_h \in \mathcal{V}_h^{**}, & (b) \end{cases} \quad (15)$$



where  $\bar{a}(u_h, v_h) = 2\mu \sum_{k=1}^{N_s} \text{meas}(\Omega_k^s) \bar{\varepsilon}^{(k)}(u_h) D_\mu \bar{\varepsilon}^{(k)}(v_h)$ ,  $\bar{b}(v_h, p_h) = \int_{\Omega} (\nabla \cdot u_h) p_h dx$ ,  $\bar{c}(p_h, q_h) = \int_{\Omega} p_h q_h dx$  and  $(f, v_h) = \int_{\Omega} f(x) v_h(x) dx$ .

## 4 The mathematical properties

Now, we show the following important properties of the bES-FEM method, when this method is applied into the linear elasticity problem:

**The first property:** The bilinear form  $\bar{a}(\cdot, \cdot)$  is continuous, symmetric and semi-elliptic on  $\mathcal{V}_{h,0}^{\mathcal{B}} := \{v \in \mathcal{V}_h^{\mathcal{B}} : \bar{b}(v, q) = 0, q \in \mathcal{V}_h^{**} \subset L_0^2(\Omega)\}$ , i.e. there exists an  $\alpha_0 > 0$  such that

$$\bar{a}(v, v) \geq \alpha_0 |v|_{\mathcal{V}_h^{\mathcal{B}}}, \quad v \in \mathcal{V}_{h,0}^{\mathcal{B}}.$$

Thanks to the theorem 3.1 in [18], it help us to prove this property.

**The second property:** The bilinear form  $\bar{b}(\cdot, \cdot)$  on  $\mathcal{V}_h^{\mathcal{B}} \times \mathcal{V}_h^{**}$  is continuous and satisfies the uniform inf-suf condition, i.e there exists a positive constant  $\beta_0$  independent the mesh size such that

$$\sup_{u_h \in \mathcal{V}_h^{\mathcal{B}}} \frac{\bar{b}(u_h, q_h)}{\|u_h\|_{\mathcal{V}_h^{\mathcal{B}}}} \geq \sup_{u_h \in \mathcal{V}_h^{\mathcal{B}}} \frac{\bar{b}(u_h, q_h)}{\|u_h\|_1} \geq \beta_0 \|q_h\|_0, \quad q_h \in \mathcal{V}_h^{**}. \quad (16)$$

*Proof*

Let  $(u_h, q_h) \in \mathcal{V}_h^{\mathcal{B}} \times \mathcal{V}_h^{**}$ , we have

$$\bar{b}(u_h, q_h) = \int_{\Omega} (\nabla \cdot u_h) q_h(x) dx = \int_{\Omega} \nabla \cdot (\ell_h + b_h) q_h(x) dx = \int_{\Omega} (\nabla \cdot \ell_h + \nabla \cdot b_h) q_h(x) dx, \quad (17)$$

where there exist uniquely  $\ell_h \in \mathcal{V}_h$  and  $b_h \in [\mathcal{B}_h]^d$  such that  $u_h = \ell_h + b_h$ . In (17), the smoothed divergences  $\nabla \cdot \ell_h$  and  $\nabla \cdot b_h$  which are restricted on  $\Omega_k^s \in \mathcal{T}_h^*$  are defined

$$(\nabla \cdot \ell_h)|_{\Omega_k^s} = \frac{1}{\text{meas}(\Omega_k^s)} \int_{\Omega_k^s} \nabla \cdot \ell_h(x) dx \text{ and } (\nabla \cdot b_h)|_{\Omega_k^s} = \frac{1}{\text{meas}(\Omega_k^s)} \int_{\Omega_k^s} \nabla \cdot b_h(x) dx.$$

To prove  $\bar{b}(u_h, q_h)$  satisfying the uniform inf-suf condition, we need to look for a relationship between  $b(u_h, q_h) = \int_{\Omega} \nabla \cdot u_h(x) q_h(x) dx$  and  $\bar{b}(u_h, q_h)$  with  $(u_h, q_h) \in \mathcal{V}_h^{\mathcal{B}} \times \mathcal{V}_h^{**}$ , because in [26] the uniform inf-suf condition holds for  $b(u_h, q_h)$ .

In the first step, we compute the value of  $\int_{\Omega} (\nabla \cdot \ell_h) q_h(x) dx - \int_{\Omega} (\nabla \cdot b_h) q_h(x) dx$  with  $(\ell_h, q_h) \in \mathcal{V}_h \times \mathcal{V}_h^{**}$ . Using the fact that  $\nabla \cdot \ell_h$  is constant on each  $T \in \mathcal{T}_h$ , we obtain

$$\int_{\Omega} \nabla \cdot \ell_h q_h(x) dx = \sum_{T \in \mathcal{T}_h} (\nabla \cdot \ell_h)|_T \int_T q_h(x) dx \quad (18)$$

At any element  $T \in \mathcal{T}_h$  with its vertices  $\{x_{T(i)}\}_{i=\overline{1,d+1}}$ , we have

$$(\nabla \cdot \ell_h)|_T \int_T q_h(x) dx = \sum_{i=1}^{d+1} \text{meas}(V_{x_{T(i)}} \cap T) \cdot q_{T(i)} = (\nabla \cdot \ell_h)|_T \sum_{i=1}^{d+1} \frac{\text{meas}(T) \cdot \text{card}(\mathcal{E}_{T(i)})}{2(d+1)} q_{T(i)}, \quad (19)$$

where for each  $i = \overline{1,d+1}$ ,  $V_{x_{T(i)}} \in \mathcal{T}_h^{**}$  is respectively associated with a vertex  $x_{T(i)}$  of  $T$ , and  $q_{T(i)}$  is a nodal value of  $q_h$  at a vertex  $x_{T(i)}$ . The value  $\text{meas}(V_{x_{T(i)}} \cap T)$  is equal to  $\frac{\text{meas}(T) \cdot \text{card}(\mathcal{E}_{T(i)})}{2(d+1)}$  with  $i = \overline{1,d+1}$ , because of the third mesh  $\mathcal{T}_h^{**}$  constructed by barycentric points of all faces, midpoints of all edges and the centroid points  $c_T$  for all  $T \in \mathcal{T}_h$ . The set  $\mathcal{E}_{T(i)}$  contains all edges of  $T$  such that these edges have a common vertex  $x_{T(i)}$ . Additionally, for all  $i = \overline{1,d}$ , the notation  $\text{card}(\mathcal{E}_{T(i)})$  which is the number of all elements of  $\mathcal{E}_{T(i)}$  is equal to  $d$ , because the primal mesh  $\mathcal{T}_h$  is a triangulation.

In (17), we consider

$$\int_{\Omega} (\nabla \cdot \ell_h) q_h(x) dx = \sum_{T \in \mathcal{T}_h} \int_T (\nabla \cdot \ell_h) \cdot q_h(x) dx \quad (20)$$

On the above element  $T \in \mathcal{T}_h$ , the integral  $\int_T (\nabla \cdot \ell_h) \cdot q_h(x) dx$  is computed by

$$\int_T (\nabla \cdot \ell_h) \cdot q_h(x) dx = \sum_{i=1}^{d+1} \left[ \sum_{e_{T(i)} \in \mathcal{E}_{T(i)}} \frac{\text{meas}(V_{x_{T(i)}} \cap T \cap \Omega_{e_{T(i)}}^s)}{\text{meas}(\Omega_{e_{T(i)}}^s)} \int_{\Omega_{e_{T(i)}}^s} \nabla \cdot \ell_h dx \right] \cdot q_{T(i)}, \quad (21)$$

where the domain  $\Omega_{e_{T(i)}}^s \in \mathcal{T}_h^*$  corresponds to the edge  $e_{T(i)}$ .

In the first case of  $T$  (a triangle or tetrahedron), we assume that all edges of  $T$  are inner edges, *i.e* the edges are not on the boundary  $\partial\Omega$ . For each  $i = \overline{1,d+1}$  and  $j = \overline{1,d}$ , the integral  $\int_{\Omega_{e_{T(i)}}^s} \nabla \cdot \ell_h dx$  is computed by

$$\int_{\Omega_{e_{T(i)}}^s} \nabla \cdot \ell_h dx = \text{meas}(\Omega_{e_{T(i)}}^s \cap T) \cdot (\nabla \cdot \ell_h)|_T + \sum_{K \in \mathcal{T}_{e_{T(i)}} \setminus \{T\}} \text{meas}(\Omega_{e_{T(i)}}^s \cap K) \cdot (\nabla \cdot \ell_h)|_K, \quad (22)$$

where the notation  $\mathcal{T}_{e_{T(i)}}$  is a subset of  $\mathcal{T}_h$  such that its elements have a common edge  $e_{T(i)}$  and  $T \in \mathcal{T}_{e_{T(i)}}$ .

From (21) and (22), the integral  $\int_T (\nabla \cdot \ell_h) \cdot q_h(x) dx$  has the coefficient of  $(\nabla \cdot \ell_h)|_T q_{T(i)}$

$$\sum_{e_{T(i)} \in \mathcal{E}_{T(i)}} \frac{\text{meas}(V_{x_{T(i)}} \cap T \cap \Omega_{e_{T(i)}}^s) \cdot \text{meas}(\Omega_{e_{T(i)}}^s \cap T)}{\text{meas}(\Omega_{e_{T(i)}}^s)}. \quad (23)$$

Together  $\int_T (\overline{\nabla \cdot \ell_h}) \cdot q_h(x) dx$ , we only find the coefficient of  $(\nabla \cdot \ell_h)|_T q_{T(i)}$  in  $\int_{K \in \mathcal{T}_{e_{T(i)}} \setminus \{T\}} (\overline{\nabla \cdot \ell_h}) \cdot q_h(x) dx$  for all  $K \in \mathcal{T}_{e_{T(i)}} \setminus \{T\}$  and  $e_{T(i)} \in \mathcal{E}_{T(i)}$ , as follows:

$$\left\{ \frac{\text{meas}\left(V_{x_{T(i)}} \cap K \cap \Omega_{e_{T(i)}}^s\right) \cdot \text{meas}\left(\Omega_{e_{T(i)}}^s \cap T\right)}{\text{meas}\left(\Omega_{e_{T(i)}}^s\right)} \right\}_{\forall K \in \mathcal{T}_{e_{T(i)}} \setminus \{T\} \text{ and } \forall e_{T(i)} \in \mathcal{E}_{T(i)}}. \quad (24)$$

From (23) and (24), in the integral  $\int_{\Omega} (\overline{\nabla \cdot \ell_h}) q_h(x) dx$ , the coefficient of  $(\nabla \cdot \ell_h)|_T q_{T(i)}$  is equal to

$$\sum_{e_{T(i)} \in \mathcal{E}_{T(i)}} \left[ \frac{\text{meas}\left(V_{x_{T(i)}} \cap T \cap \Omega_{e_{T(i)}}^s\right) \cdot \text{meas}\left(\Omega_{e_{T(i)}}^s \cap T\right)}{\text{meas}\left(\Omega_{e_{T(i)}}^s\right)} + \sum_{K \in \mathcal{T}_{e_{T(i)}} \setminus \{T\}} \frac{\text{meas}\left(V_{x_{T(i)}} \cap K \cap \Omega_{e_{T(i)}}^s\right) \cdot \text{meas}\left(\Omega_{e_{T(i)}}^s \cap T\right)}{\text{meas}\left(\Omega_{e_{T(i)}}^s\right)} \right]. \quad (25)$$

By using the centroids  $c_T$  for all  $T \in \mathcal{T}_h$ , the midpoints of all edges, plus barycentric points of all faces (3D) to construct the dual mesh  $\mathcal{T}_h^*$  and the third mesh  $\mathcal{T}_h^{**}$ , we have

$$\begin{aligned} \text{meas}\left(V_{x_{T(i)}} \cap T \cap \Omega_{e_{T(i)}}^s\right) &= \frac{\text{meas}(T)}{2(d+1)}, \text{meas}\left(V_{x_{T(i)}} \cap K \cap \Omega_{e_{T(i)}}^s\right) = \frac{\text{meas}(K)}{2(d+1)}, \\ \text{meas}\left(\Omega_{e_{T(i)}}^s \cap T\right) &= \frac{\text{meas}(T)}{d+1}, \text{meas}\left(\Omega_{e_{T(i)}}^s\right) = \sum_{L \in \mathcal{T}_{e_{T(i)}}} \frac{\text{meas}(L)}{d+1}. \end{aligned} \quad (26)$$

Therefore, the coefficient of  $(\nabla \cdot v_h)|_T q_{T(i)}$  is computed by

$$\frac{\text{meas}(T)}{d+1} \cdot \sum_{e_{T(i)} \in \mathcal{E}_{T(i)}} \left[ \frac{\frac{\text{meas}(T)}{2(d+1)}}{\sum_{L \in \mathcal{T}_{e_{T(i)}}} \frac{\text{meas}(L)}{d+1}} + \sum_{K \in \mathcal{T}_{e_{T(i)}} \setminus \{T\}} \frac{\frac{\text{meas}(K)}{2(d+1)}}{\sum_{L \in \mathcal{T}_{e_{T(i)}}} \frac{\text{meas}(L)}{d+1}} \right] = \frac{\text{meas}(T) \cdot \text{card}(\mathcal{E}_{T(i)})}{2(d+1)}. \quad (27)$$

From (19) and (27), the two coefficients of  $(\nabla \cdot \ell_h)|_T q_{T(i)}$  in the two integrals  $\int_{\Omega} (\overline{\nabla \cdot \ell_h}) q_h(x) dx$  and  $\int_{\Omega} (\nabla \cdot \ell_h) q_h(x) dx$  are together equal.

In the other cases of  $T$ , it has least one edge belonging to the boundary  $\partial\Omega$ , we also obtain the same results. Hence, the value of  $\int_{\Omega} (\overline{\nabla \cdot \ell_h}) q_h(x) dx - \int_{\Omega} (\nabla \cdot \ell_h) q_h(x) dx$  is equal to 0. According to the result of [26], without enriching the displacement space, the uniform inf-sup condition is violated.

In the second step, we find the relationship between  $\int_{\Omega} (\overline{\nabla \cdot b_h}) q_h(x) dx$  and  $\int_{\Omega} (\nabla \cdot b_h) q_h(x) dx$ . Using the definitions of the spaces  $\mathcal{B}_h$  and  $\mathcal{V}_h^{**}$ , with  $(b_h, q_h) \in \mathcal{B}_h \times \mathcal{V}_h^{**}$ , we get

$$\int_{\Omega} \nabla \cdot b_h(x) q_h(x) dx = \sum_{T \in \mathcal{T}_h} \sum_{\substack{i=1, V_i \in \mathcal{T}_h^* \\ T \cap V_i \neq \emptyset}}^{N_n} \left[ \int_{V_i \cap T} \nabla \cdot b_h(x) q_i dx \right] \quad (28)$$

and

$$\int_{\Omega} \overline{\nabla \cdot b_h(x)} q_h(x) dx = \sum_{T \in \mathcal{T}_h} \sum_{\substack{i=1, V_i \in \mathcal{T}_h^* \\ T \cap V_i \neq \emptyset}}^{N_n} \left[ \int_{V_i \cap T} \overline{\nabla \cdot b_h(x)} q_i dx \right] \quad (29)$$

Considering  $T$  whose all edges stay in the internal domain  $\Omega$ , for each  $i = \overline{1, d+1}$ , we have

$$\int_{V_{x_{T(i)}} \cap T} \nabla \cdot b_h(x) q_{T(i)} dx = q_{T(i)} u_{c_T} \cdot \int_{V_{x_{T(i)}} \cap T} \nabla N_{c_T}^b(x) dx, \quad (30)$$

where  $b_h$  is rewritten as  $b_h = u_{c_T} N_{c_T}^b$  with a vector  $u_{c_T}$ , and

$$\begin{aligned} \int_{V_{x_{T(i)}} \cap T} \overline{\nabla \cdot b_h(x)} q_{T(i)} dx &= \left[ \sum_{e_{T(i)} \in \mathcal{E}_{T(i)}} \text{meas} \left( V_{x_{T(i)}} \cap T \cap \Omega_{e_{T(i)}}^s \right) (\nabla \cdot b_h)|_{\Omega_{e_{T(i)}}^s} \right] q_{T(i)} \\ &= \left\{ \sum_{e_{T(i)} \in \mathcal{E}_{T(i)}} \frac{\text{meas} \left( V_{x_{T(i)}} \cap T \cap \Omega_{e_{T(i)}}^s \right)}{\text{meas} \left( \Omega_{e_{T(i)}}^s \right)} \cdot \left[ \sum_{K \in \mathcal{T}_{e_{T(i)}} \subset \mathcal{T}_h^*} \left( \int_{\Omega_{e_{T(i)}}^s \cap K} \nabla \cdot b_h(x) dx \right) \right] \right\} q_{T(i)} \\ &= \left\{ \sum_{e_{T(i)} \in \mathcal{E}_{T(i)}} \frac{\text{meas} \left( V_{x_{T(i)}} \cap T \cap \Omega_{e_{T(i)}}^s \right)}{\text{meas} \left( \Omega_{e_{T(i)}}^s \right)} \cdot \left[ \sum_{K \in \mathcal{T}_{e_{T(i)}} \subset \mathcal{T}_h^*} u_{c_K} \cdot \left( \int_{\Omega_{e_{T(i)}}^s \cap K} \nabla N_{c_K}^b(x) dx \right) \right] \right\} q_{T(i)}. \end{aligned} \quad (31)$$

From (31), in the integral  $\int_{V_{x_{T(i)}} \cap T} (\overline{\nabla \cdot b_h}) q_{T(i)} dx$ , the coefficient of  $q_{T(i)} u_{c_T}$  with  $T \in \mathcal{T}_{e_{T(i)}}$  is equal to

$$\sum_{e_{T(i)} \in \mathcal{E}_{T(i)}} \left[ \frac{\text{meas} \left( V_{x_{T(i)}} \cap T \cap \Omega_{e_{T(i)}}^s \right)}{\text{meas} \left( \Omega_{e_{T(i)}}^s \right)} \int_{\Omega_{e_{T(i)}}^s \cap T} \nabla N_{c_T}^b(x) dx \right]. \quad (32)$$

Furthermore, the other coefficients of  $q_{T(i)} u_{c_T}$ , which are also found in

$$\left\{ \int_{V_{x_{T(i)}} \cap K} (\nabla \cdot b_h) q_{T(i)} \right\}_{K \in \{ \mathcal{T}_{e_{T(i)}} \setminus T \} \subset \mathcal{T}_h, \forall e_{T(i)} \in \mathcal{E}_{T(i)}},$$

are equal to

$$\left\{ \frac{\text{meas}\left(V_{x_{T(i)}} \cap K \cap \Omega_{e_{T(i)}}^s\right)}{\text{meas}\left(\Omega_{e_{T(i)}}^s\right)} \int_{\Omega_{e_{T(i)}}^s \cap T} \nabla N_{c_T}^b(x) dx \right\}_{\substack{K \in \{\mathcal{T}_{e_{T(i)}} \setminus T\} \subset \mathcal{T}_h \\ \forall e_{T(i)} \in \mathcal{E}_{T(i)}}} . \quad (33)$$

Thank to (26), (32) and (33), the coefficient of  $q_{T(i)} u_{c_T}$  are computed in the integral  $\int_{\Omega} (\nabla \cdot \overline{b_h}) q_h(x) dx$ , as follows:

$$\begin{aligned} & \sum_{e_{T(i)} \in \mathcal{E}_{T(i)}} \left\{ \frac{\text{meas}\left(V_{x_{T(i)}} \cap T \cap \Omega_{e_{T(i)}}^s\right)}{\text{meas}\left(\Omega_{e_{T(i)}}^s\right)} + \sum_{K \in \{\mathcal{T}_{e_{T(i)}} \setminus T\} \subset \mathcal{T}_h} \left[ \frac{\text{meas}\left(V_{x_{T(i)}} \cap K \cap \Omega_{e_{T(i)}}^s\right)}{\text{meas}\left(\Omega_{e_{T(i)}}^s\right)} \right] \right\} \int_{\Omega_{e_{T(i)}}^s \cap T} \nabla N_{c_T}^b(x) dx \\ &= \sum_{e_{T(i)} \in \mathcal{E}_{T(i)}} \left[ \frac{\frac{\text{meas}(T)}{2(d+1)}}{\sum_{L \in \mathcal{T}_{e_{T(i)}}} \frac{\text{meas}(L)}{d+1}} + \sum_{K \in \{\mathcal{T}_{e_{T(i)}} \setminus T\} \subset \mathcal{T}_h} \left( \frac{\frac{\text{meas}(K)}{2(d+1)}}{\sum_{L \in \mathcal{T}_{e_{T(i)}}} \frac{\text{meas}(L)}{d+1}} \right) \right] \int_{\Omega_{e_{T(i)}}^s \cap T} \nabla N_{c_T}^b(x) dx \\ &= \frac{1}{2} \sum_{e_{T(i)} \in \mathcal{E}_{T(i)}} \left( \int_{\Omega_{e_{T(i)}}^s \cap T} \nabla N_{c_T}^b(x) dx \right). \quad (34) \end{aligned}$$

In two dimensions, we compute the coefficient of  $q_{T(i)} u_{c_T}$  (34) on the following triangle  $T$  having three vertices  $\{x_i, x_j, x_k\}$

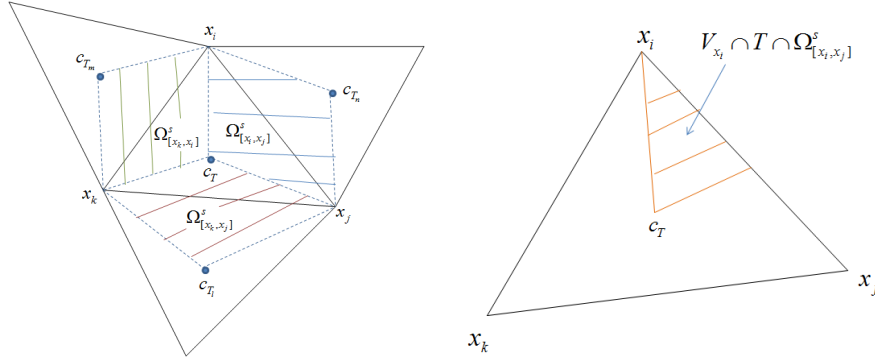


Figure 5

This coefficient is equal to

$$\frac{1}{2} \left( \int_{\Omega_{[x_i, x_j]}^s \cap T} \nabla N_{c_T}^b(x) dx + \int_{\Omega_{[x_k, x_i]}^s \cap T} \nabla N_{c_T}^b(x) dx \right) = \frac{1}{2} \left( \int_{\gamma_j^{(1)}} N_{c_T}^b(x) n_{\gamma_j^{(1)}} dx + \int_{\gamma_k^{(1)}} N_{c_T}^b(x) n_{\gamma_k^{(1)}} dx \right), \quad (35)$$

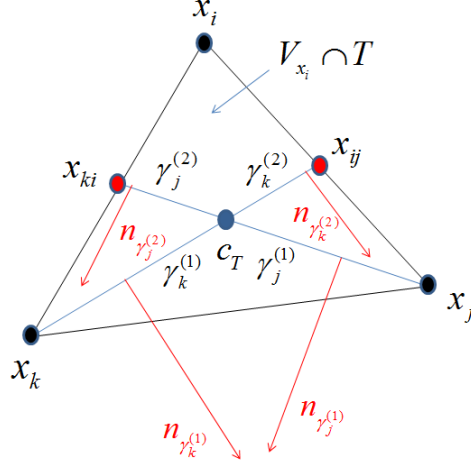


Figure 6

In Figure 6, we introduce some extra notations including that the midpoints of edges  $[x_i, x_j]$ ,  $[x_k, x_i]$  and  $[x_k, x_j]$  are denoted by  $x_{ij}$ ,  $x_{ki}$  and  $x_{kj}$ . Besides, notations  $\gamma_k^{(1)}$ ,  $\gamma_k^{(2)}$ ,  $\gamma_j^{(1)}$  and  $\gamma_j^{(2)}$  are edges  $[x_k, c_T]$ ,  $[x_{ij}, c_T]$ ,  $[x_j, c_T]$  and  $[x_{ki}, c_T]$ . Vectors  $n_{\gamma_k^{(1)}}$ ,  $n_{\gamma_k^{(2)}}$ ,  $n_{\gamma_j^{(1)}}$  and  $n_{\gamma_j^{(2)}}$  are outward normal vectors of  $\Omega_{[x_i, x_j]}^s \cap T$ ,  $\Omega_{[x_k, x_i]}^s \cap T$  and  $V_{x_i} \cap T$ , respectively. Length of each vector  $n_{\gamma_k^{(1)}}$ ,  $n_{\gamma_k^{(2)}}$ ,  $n_{\gamma_j^{(1)}}$  and  $n_{\gamma_j^{(2)}}$  is equal length of each segment  $\gamma_k^{(1)}$ ,  $\gamma_k^{(2)}$ ,  $\gamma_j^{(1)}$  and  $\gamma_j^{(2)}$ , so  $n_{\gamma_k^{(1)}} = 2n_{\gamma_k^{(2)}}$  and  $n_{\gamma_j^{(1)}} = 2n_{\gamma_j^{(2)}}$ , because length of each segment  $\gamma_k^{(1)}$ ,  $\gamma_j^{(1)}$  is equal two times length of each segment  $\gamma_k^{(2)}$ ,  $\gamma_j^{(2)}$ , respectively.

We directly compute the coefficient (35) in the following two types of bubble functions

■ *The  $\xi$ -th-power bubble functions (9) with  $\xi = 3$  (the cubic bubble functions)*

Assume that  $\hat{T}$  is the reference triangle,  $M_T$  is the Jacobian of transformation from the triangle  $T$  to  $\hat{T}$ ,  $J_T = \det(M_T)$ ,  $\hat{\theta}_2^{(1)} = \int_{\hat{\gamma}_2^{(1)}} N_{c_{\hat{T}}}^b(x) dx$ ,  $\hat{\theta}_2^{(2)} = \int_{\hat{\gamma}_2^{(2)}} N_{c_{\hat{T}}}^b(x) dx$ ,  $\hat{\theta}_3^{(1)} = \int_{\hat{\gamma}_3^{(1)}} N_{c_{\hat{T}}}^b(x) dx$  and  $\hat{\theta}_3^{(2)} = \int_{\hat{\gamma}_3^{(2)}} N_{c_{\hat{T}}}^b(x) dx$ , where notations  $\hat{\gamma}_i^{(j)}$  are defined

$$\hat{\gamma}_1^{(1)} = [x_{\hat{T}(1)}, c_{\hat{T}}], \quad \hat{\gamma}_1^{(2)} = [x_{\hat{T}(23)}, c_{\hat{T}}], \quad \hat{\gamma}_2^{(1)} = [x_{\hat{T}(2)}, c_{\hat{T}}],$$

$$\hat{\gamma}_2^{(2)} = [x_{\hat{T}(13)}, c_{\hat{T}}], \quad \hat{\gamma}_3^{(1)} = [x_{\hat{T}(3)}, c_{\hat{T}}], \quad \hat{\gamma}_3^{(2)} = [x_{\hat{T}(12)}, c_{\hat{T}}]$$

with points  $x_{\hat{T}(1)}(0, 1)$ ,  $x_{\hat{T}(2)}(0, 0)$ ,  $x_{\hat{T}(3)}(1, 0)$ ,  $x_{\hat{T}(12)}(0, \frac{1}{2})$ ,  $x_{\hat{T}(23)}(\frac{1}{2}, 0)$ ,  $x_{\hat{T}(13)}(\frac{1}{2}, \frac{1}{2})$  and  $c_{\hat{T}}(\frac{1}{3}, \frac{1}{3})$ .

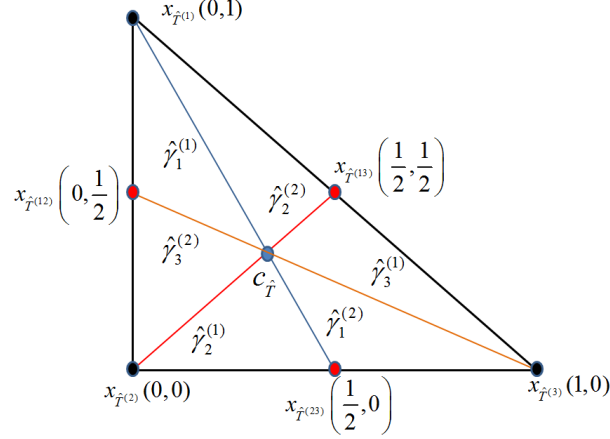


Figure 7

Together this assumption, we use the lemma 3.2 of [26] to obtain

$$\int_{\gamma_j^{(1)}} N_{c_T}^b(x) n_{\gamma_j^{(1)}} dx + \int_{\gamma_k^{(1)}} N_{c_T}^b(x) n_{\gamma_k^{(1)}} dx = J_T \left( \hat{\theta}_{\hat{\gamma}_2^{(1)}} \hat{n}_{\hat{\gamma}_2^{(1)}} + \hat{\theta}_{\hat{\gamma}_3^{(1)}} \hat{n}_{\hat{\gamma}_3^{(1)}} \right) M_T^{-1}. \quad (36)$$

$$\int_{V_{x_i} \cap T} \nabla N_{c_T}^b(x) dx = J_T \left( \hat{\theta}_{\hat{\gamma}_2^{(2)}} \hat{n}_{\hat{\gamma}_2^{(2)}} + \hat{\theta}_{\hat{\gamma}_3^{(2)}} \hat{n}_{\hat{\gamma}_3^{(2)}} \right) M_T^{-1}. \quad (37)$$

By directly computing the quantities on the reference element  $\hat{T}$ , we have

- The barycentric coordinates of a point  $P(x^{(1)}, x^{(2)})$  in the reference triangle  $\hat{T}$  are  $\hat{\lambda}_1(x) = x^{(2)}$ ,  $\hat{\lambda}_2(x) = 1 - x^{(1)} - x^{(2)}$  and  $\hat{\lambda}_3(x) = x^{(1)}$  with  $x = (x^{(1)}, x^{(2)})$ . The basic cubic bubble function on the reference triangle  $\hat{T}$  is  $N_{c_{\hat{T}}}^b(x) = 27 \cdot \lambda_1(x) \cdot \lambda_2(x) \cdot \lambda_3(x)$ .
- The segments  $\hat{\gamma}_1^{(1)}$ ,  $\hat{\gamma}_1^{(2)}$  are on the line  $(d_1) x^{(2)} = -2x^{(1)} + 1$ .
- The segments  $\hat{\gamma}_2^{(1)}$ ,  $\hat{\gamma}_2^{(2)}$  are on the line  $(d_2) x^{(2)} = x^{(1)}$ .
- The segments  $\hat{\gamma}_3^{(1)}$ ,  $\hat{\gamma}_3^{(2)}$  are on the line  $(d_3) x^{(2)} = -0.5x^{(1)} + 0.5$ .
- The values of the following integrals:

$$\begin{aligned} \hat{\theta}_{\hat{\gamma}_1^{(1)}} &= \int_{\hat{\gamma}_1^{(1)}} N_{c_T}^b(x) d\gamma(x) = 27 \int_0^{1/3} s^2 (1 - 2s) \sqrt{5} ds = \frac{\sqrt{5}}{6}, \\ \hat{\theta}_{\hat{\gamma}_1^{(2)}} &= \int_{\hat{\gamma}_1^{(2)}} N_{c_T}^b(x) d\gamma(x) = 27 \int_{1/3}^{1/2} s^2 (1 - 2s) \sqrt{5} ds = \frac{11 \cdot \sqrt{5}}{96}, \quad \hat{\theta}_{\hat{\gamma}_1^{(1)}} = \frac{16}{11} \hat{\theta}_{\hat{\gamma}_1^{(2)}}. \end{aligned} \quad (38)$$

$$\begin{aligned}
\hat{\theta}_{\hat{\gamma}_2^{(1)}} &= \int_{\hat{\gamma}_2^{(1)}} N_{c_T}^b(x) d\gamma(x) = 27 \int_0^{1/3} s^2(1-2s)\sqrt{2} ds = \frac{27\sqrt{2}}{162}, \\
\hat{\theta}_{\hat{\gamma}_2^{(2)}} &= \int_{\hat{\gamma}_2^{(2)}} N_{c_T}^b(x) d\gamma(x) = 27 \int_{1/3}^{1/2} s^2(1-2s)\sqrt{2} ds = \frac{11 \cdot 27 \cdot \sqrt{2}}{2592}, \quad \hat{\theta}_{\hat{\gamma}_2^{(1)}} = \frac{16}{11} \hat{\theta}_{\hat{\gamma}_2^{(2)}}.
\end{aligned} \tag{39}$$

$$\begin{aligned}
\hat{\theta}_{\hat{\gamma}_3^{(1)}} &= \int_{\hat{\gamma}_3^{(1)}} N_{c_T}^b(x) d\gamma(x) = 27 \int_{1/3}^1 s(0.5-0.5s)^2 \sqrt{1+0.25} ds = \frac{16 \cdot \sqrt{1.25}}{48} \\
\hat{\theta}_{\hat{\gamma}_3^{(2)}} &= \int_{\hat{\gamma}_3^{(2)}} N_{c_T}^b(x) d\gamma(x) = 27 \int_0^{1/3} s(0.5-0.5s)^2 \sqrt{1+0.25} ds = \frac{11 \cdot \sqrt{1.25}}{48}, \quad \hat{\theta}_{\hat{\gamma}_3^{(1)}} = \frac{16}{11} \hat{\theta}_{\hat{\gamma}_3^{(2)}}
\end{aligned} \tag{40}$$

- The relationships between the normal vectors  $n_{\hat{\gamma}_i^{(1)}}$  and  $n_{\hat{\gamma}_i^{(2)}}$  with  $i = \overline{1, 3}$ :

$$n_{\hat{\gamma}_1^{(1)}} = 2n_{\hat{\gamma}_1^{(2)}}, \quad n_{\hat{\gamma}_2^{(1)}} = 2n_{\hat{\gamma}_2^{(2)}} \quad \text{and} \quad n_{\hat{\gamma}_3^{(1)}} = 2n_{\hat{\gamma}_3^{(2)}}. \tag{41}$$

From (36)-(41), we point out that

$$\int_{\Omega_{[x_i, x_j]}^s \cap T} \nabla N_{c_T}^b(x) dx + \int_{\Omega_{[x_k, x_i]}^s \cap T} \nabla N_{c_T}^b(x) dx = \frac{32}{11} \int_{V_{x_i} \cap T} \nabla N_{c_T}^b(x) dx. \tag{42}$$

Hence, we use the results of (30), (35) and (42) to imply that

$$\text{the coefficient of } p_{T^{(i)}} u_{c_T} \text{ in } \bar{b}(u_h, p_h) = \frac{16}{11} \cdot \text{the coefficient of } p_{T^{(i)}} u_{c_T} \text{ in } b(u_h, p_h). \tag{43}$$

With computations of (28), (29) and (43), we conclude that

$$\int_{\Omega} (\overline{\nabla \cdot b_h}) q_h(x) dx = \frac{16}{11} \int_{\Omega} (\nabla \cdot b_h) q_h(x) dx, \tag{44}$$

Defining  $u_h^* = \ell_h + \frac{11}{16} b_h$ , using (44) and the result of the first step, we get

$$\int_{\Omega} (\overline{\nabla \cdot u_h^*}) q_h(x) dx = \int_{\Omega} (\nabla \cdot u_h) q_h(x) dx. \tag{45}$$

Finally, thank to the result of Theorem 3.1 of [26] and (45), the uniform inf-suf condition holds for the bilinear form  $\bar{b}(\cdot, \cdot)$  on  $\mathcal{V}_h^B \times \mathcal{V}_h^{**}$ .

■ *The hat bubble functions (10)*



For each triangle  $T \in \mathcal{T}_h$ , the divergence of hat bubble functions is equal to constant on each sub-triangle  $\{T_{(i)}\}_{i=1,3}$  of  $T$ , so we get

$$\int_{\Omega_{[x_i, x_j]}^s \cap T} \nabla N_{c_T}^b(x) dx + \int_{\Omega_{[x_k, x_i]}^s \cap T} \nabla N_{c_T}^b(x) dx = \frac{1}{2} \int_{V_{x_i} \cap T} \nabla N_{c_T}^b(x) dx. \quad (46)$$

By (30), (35) and (46), we obtain

$$\text{the coefficient of } p_{T(i)} u_{c_T} \text{ in } \bar{b}(u_h, p_h) = \text{the coefficient of } p_{T(i)} u_{c_T} \text{ in } b(u_h, p_h), \quad (47)$$

which implies that

$$\int_{\Omega} (\overline{\nabla \cdot b_h}) q_h(x) dx = \int_{\Omega} (\nabla \cdot b_h) q_h(x) dx. \quad (48)$$

Therefore,

$$\int_{\Omega} (\overline{\nabla \cdot u_h}) q_h(x) dx = \int_{\Omega} (\nabla \cdot u_h) q_h(x) dx. \quad (49)$$

In three dimensions, we also compute the coefficient of  $q_{T(i)} u_{c_T}$  (34) on the following tetrahedron  $T$  constructed from four vertices  $\{x_{T(1)}, x_{T(2)}, x_{T(3)}, x_{T(4)}\}$ ,

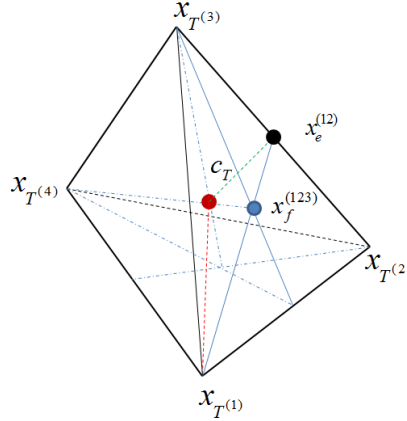


Figure 8

where  $c_T$  is the centroid of  $T$ ,  $x_f^{(ijk)}$  is the barycentric point of the triangular face  $(x_{T(i)}, x_{T(j)}, x_{T(k)})$ ,  $x_e^{(ij)}$  is the midpoint of the edge  $[x_{T(i)}, x_{T(j)}]$ , where  $i, j, k$  belong to  $\{1, 2, 3, 4\}$ .

In particular case, the detailed coefficient of  $q_{T(i)}u_{c_T}$  (34) of  $\bar{b}(u, q)$  is computed as

$$\begin{aligned}
& \frac{1}{2} \left( \int_{\Omega^s_{[x_{T(i)}, x_{T(j)}]} \cap T} \nabla N_{c_T}^b(x) dx + \int_{\Omega^s_{[x_{T(i)}, x_{T(k)}]} \cap T} \nabla N_{c_T}^b(x) dx + \int_{\Omega^s_{[x_{T(i)}, x_{T(l)}]} \cap T} \nabla N_{c_T}^b(x) dx \right) \\
&= \frac{1}{2} \left( \int_{(c_T, x_f^{(ijk)}, x_{T(j)})} N_{c_T}^b(x) n_{(c_T, x_f^{(ijk)}, x_{T(j)})} d\gamma(x) + \int_{(c_T, x_f^{(ijl)}, x_{T(j)})} N_{c_T}^b(x) n_{(c_T, x_f^{(ijl)}, x_{T(j)})} d\gamma(x) + \right. \\
&\quad \int_{(c_T, x_f^{(ijk)}, x_{T(k)})} N_{c_T}^b(x) n_{(c_T, x_f^{(ijk)}, x_{T(k)})} d\gamma(x) + \int_{(c_T, x_f^{(ikl)}, x_{T(k)})} N_{c_T}^b(x) n_{(c_T, x_f^{(ikl)}, x_{T(k)})} d\gamma(x) + \\
&\quad \left. \int_{(c_T, x_f^{(ijl)}, x_{T(l)})} N_{c_T}^b(x) n_{(c_T, x_f^{(ijl)}, x_{T(l)})} d\gamma(x) + \int_{(c_T, x_f^{(ikl)}, x_{T(l)})} N_{c_T}^b(x) n_{(c_T, x_f^{(ikl)}, x_{T(l)})} d\gamma(x) \right) \quad (50)
\end{aligned}$$

where  $j, k, l \in \{1, 2, 3, 4\}$  are different from  $i$ . Vectors  $n_{(c_T, x_f^{(ijk)}, x_{T(j)})}$ ,  $n_{(c_T, x_f^{(ijl)}, x_{T(j)})}$ ,  $n_{(c_T, x_f^{(ijk)}, x_{T(k)})}$ ,  $n_{(c_T, x_f^{(ikl)}, x_{T(k)})}$ ,  $n_{(c_T, x_f^{(ijl)}, x_{T(l)})}$ ,  $n_{(c_T, x_f^{(ikl)}, x_{T(l)})}$  whose length is equal to measure of triangular faces  $(c_T, x_f^{(ijk)}, x_{T(j)})$ ,  $(c_T, x_f^{(ijl)}, x_{T(j)})$ ,  $(c_T, x_f^{(ijk)}, x_{T(k)})$ ,  $(c_T, x_f^{(ikl)}, x_{T(k)})$ ,  $(c_T, x_f^{(ijl)}, x_{T(l)})$  and  $(c_T, x_f^{(ikl)}, x_{T(l)})$  respectively, are the outward normal vectors of  $T$ .

Moreover, we also have the coefficient of  $q_{T(i)}u_{c_T}$  of  $b(u, q)$ , as follows:

$$\left( \int_{(c_T, x_f^{(ijk)}, x_e^{(i,j)})} N_{c_T}^b(x) n_{(c_T, x_f^{(ijk)}, x_e^{(i,j)})} d\gamma(x) + \int_{(c_T, x_f^{(ijl)}, x_e^{(i,j)})} N_{c_T}^b(x) n_{(c_T, x_f^{(ijl)}, x_e^{(i,j)})} d\gamma(x) + \right. \\
\int_{(c_T, x_f^{(ijk)}, x_e^{(i,k)})} N_{c_T}^b(x) n_{(c_T, x_f^{(ijk)}, x_e^{(i,k)})} d\gamma(x) + \int_{(c_T, x_f^{(ikl)}, x_e^{(i,k)})} N_{c_T}^b(x) n_{(c_T, x_f^{(ikl)}, x_e^{(i,k)})} d\gamma(x) + \\
\left. \int_{(c_T, x_f^{(ijl)}, x_e^{(i,l)})} N_{c_T}^b(x) n_{(c_T, x_f^{(ijl)}, x_e^{(i,l)})} d\gamma(x) + \int_{(c_T, x_f^{(ikl)}, x_e^{(i,l)})} N_{c_T}^b(x) n_{(c_T, x_f^{(ikl)}, x_e^{(i,l)})} d\gamma(x) \right) \quad (51)$$

Furthermore, we have relationships between normal vectors in the two formulas (50) and (51)

$$\begin{aligned}
n_{(c_T, x_f^{(ijk)}, x_{T(j)})} &= 2n_{(c_T, x_f^{(ijk)}, x_e^{(i,j)})}, n_{(c_T, x_f^{(ijl)}, x_{T(j)})} = 2n_{(c_T, x_f^{(ijl)}, x_e^{(i,j)})}, \\
n_{(c_T, x_f^{(ijk)}, x_{T(k)})} &= 2n_{(c_T, x_f^{(ijk)}, x_e^{(i,k)})}, n_{(c_T, x_f^{(ikl)}, x_{T(k)})} = 2n_{(c_T, x_f^{(ikl)}, x_e^{(i,k)})}, \\
n_{(c_T, x_f^{(ijl)}, x_{T(l)})} &= 2n_{(c_T, x_f^{(ijl)}, x_e^{(i,l)})}, n_{(c_T, x_f^{(ikl)}, x_{T(l)})} = 2n_{(c_T, x_f^{(ikl)}, x_e^{(i,l)})} \quad (52)
\end{aligned}$$

Obviously, from (50), (51) and (52), if the hat bubble function  $N_{c_T}^b$  is considered, we also get

$$\text{the coefficient of } p_{T(i)}u_{c_T} \text{ in } \bar{b}(u_h, p_h) = \text{the coefficient of } p_{T(i)}u_{c_T} \text{ in } b(u_h, p_h), \quad (53)$$

which leads to

$$\int_{\Omega} (\overline{\nabla \cdot b_h}) q_h(x) dx = \int_{\Omega} (\nabla \cdot b_h) q_h(x) dx. \quad (54)$$

Hence,

$$\int_{\Omega} (\overline{\nabla \cdot u_h}) q_h(x) dx = \int_{\Omega} (\nabla \cdot u_h) q_h(x) dx. \quad (55)$$

With the 4th-bubble functions  $N_{c_T}^b$ , there exists a positive constant  $\alpha$  such that

$$\int_{\Omega} (\overline{\nabla \cdot u_h^*}) q_h(x) dx = \int_{\Omega} (\nabla \cdot u_h) q_h(x) dx. \quad (56)$$

with  $u_h = \ell_h + b_h$  and  $u_h^* = \ell_h + \alpha b_h$  in  $\Omega$ .

**The third property:** The bilinear form  $c(.,.)$  is continuous, symmetric and positive semidefinite, i.e

$$\bar{c}(q, q) \geq 0, \quad q \in L_0^2(\Omega).$$

**Remark 4.1:** From (15b), we can compute the pressure field by the displacement based on the edge-based smoothing domains, as follows:

$$\int_{\Omega} p_h q_h dx = \lambda \int_{\Omega} (\overline{\nabla u_h}) q_h dx$$

For each  $i = \overline{i, N_n}$ , we choose  $q_h = \chi_i$ , where  $\chi_i$  is a characteristic function of  $V_i \in \mathcal{T}_h^{**}$ . It follows that

$$p_i = \frac{\lambda}{\text{meas}(V_i)} \sum_{\substack{k=1, \Omega_k^s \in \mathcal{T}_h^* \\ \Omega_k^s \cap V_i \neq \emptyset}}^{N_s} \text{meas}(V_i \cap \Omega_k^s) (\overline{\nabla \cdot u_h})|_{\Omega_k^s}, \quad (57)$$

where  $p_h = \sum_{i=1}^{N_n} p_i \chi_i$ ,  $\chi_i \cdot \chi_j = 0$  with  $i \neq j$ . Then the bilinear  $\bar{b}(v_h, p_h)$  can be transformed into

$$\bar{b}(v_h, p_h) = \lambda \sum_{i=1}^{N_n} \frac{1}{\text{meas}(V_i)} \left( \sum_{\substack{k=1, \Omega_k^s \in \mathcal{T}_h^* \\ \Omega_k^s \cap V_i \neq \emptyset}}^{N_s} \text{meas}(V_i \cap \Omega_k^s) (\overline{\nabla \cdot u})|_{\Omega_k^s} \right) \left( \sum_{\substack{l=1, \Omega_l^s \in \mathcal{T}_h^* \\ \Omega_l^s \cap V_i \neq \emptyset}}^{N_s} \text{meas}(V_i \cap \Omega_l^s) (\overline{\nabla \cdot v})|_{\Omega_l^s} \right) \quad (58)$$

Therefore, we arrive at a problem of finding  $u_h \in \mathcal{V}_h^{\mathcal{B}}$  such that

$$\begin{aligned}
& \bar{a}(u_h, v_h) + \\
& \sum_{i=1}^{N_n} \frac{\lambda}{\text{meas}(V_i)} \left( \sum_{\substack{k=1, \Omega_k^s \in T_h^* \\ \Omega_k^s \cap V_i \neq \emptyset}}^{N_s} \text{meas}(V_i \cap \Omega_k^s) (\nabla \cdot u)|_{\Omega_k^s} \right) \left( \sum_{\substack{l=1, \Omega_l^s \in T_h^* \\ \Omega_l^s \cap V_i \neq \emptyset}}^{N_s} \text{meas}(V_i \cap \Omega_l^s) (\nabla \cdot v)|_{\Omega_l^s} \right) \\
& = (f, v_h) \quad \forall v_h \in \mathcal{V}_h^{\mathcal{B}},
\end{aligned} \tag{59}$$

where the solution  $u_h$  of (59) is the same as the solution of the problem (15).

**Remark 4.2:** For applying the bES-FEM scheme into the linear elasticity problem, the algebraic formulation of the problem is written as

$$\begin{pmatrix} A & B^T \\ B & -\frac{1}{\lambda}C \end{pmatrix} \begin{pmatrix} u_h \\ p_h \end{pmatrix} = \begin{pmatrix} f_h \\ 0 \end{pmatrix}, \tag{60}$$

where  $A$ ,  $B$ ,  $C$  are matrices associated with the bilinear form as  $\bar{a}(\cdot, \cdot)$ ,  $\bar{b}(\cdot, \cdot)$  and  $\bar{c}(\cdot, \cdot)$ , respectively, and  $f_h$  is associated with the linear operator  $(f, \cdot)$ . This framework of the bES-FEM scheme implementing in the linear elasticity problem is as in the case of the mini scheme. However, the matrix  $C$  of (60) is different from the associated matrix of the mini scheme, because the matrix  $C$  of (60) is diagonal and each degree of freedom corresponding to the pressure can be computed by (57). It follows that the matrix is positive definite.

## 5 Error norms

Here, we introduce the notations of the well-known methods used to compare with the bES-FEM method—the edge based smooth finite element method enriched by bubble functions. The list of these notations includes

- MINI - The mixed displacement/pressure finite element method with cubic bubble functions [2].
- FEM - The standard FEM using three node triangular element with shape linear function [29].
- NS-FEM - The node-based SFEM [22] using triangular elements.
- ES-FEM - The edge-based SFEM [23] using triangular elements.
- ASOI - Assumed strain stabilization using the OI strain field [45].
- ASQBI - Assumed strain stabilization using the QBI strain field [45].
- ASMD - Assumed strain stabilization using the strain field associated with the mean dilatation element [45].
- SRI - The selective-reduced integration element [11].

Furthermore, for studying the error and convergence rate of above numerical methods, we offer three types of error norms consisting of the displacement error norm and the pressure norm.

- *Displacement error norm*

The displacement error norm is defined by

$$\|u - u_h\|_{L^2(\Omega)} = \left[ \sum_{T \in \mathcal{T}_h} \int_T (u - u_h)^T (u - u_h) dx \right]^{1/2}, \quad (61)$$

where  $u$  is the analytical solution for the displacement and  $u_h$  is the approximate solution for the displacement of any numerical methods.

- *Pressure error norm*

We also have the following definition for the pressure error norm

$$\|p - p_h\|_{L^2(\Omega)} = \left[ \sum_{V \in \mathcal{T}_h^{**}} \int_V (p - p_h)^2 dx \right]^{1/2}, \quad (62)$$

where  $p, p_h$  are the analytical pressure solution and the numerical pressure solution, respectively.

- *Energy error norm*

Recalling that we only use and approximate the displacement field in the NS-FEM method, but in the the MINI and bES-FEM methods, these method have not only the displacement variable but also the extra discrete pressure variable. Hence, we propose a different definition of the energy error norm for each method, as follows:

For the NS-FEM, ES-FEM methods, the evaluation of the energy error norm is based on  $N_s$  smoothing domain  $\Omega_k^s \in \mathcal{T}_h^*$ , so it is defined as in [18]

$$\|u - u_h\|_E = \left\{ \sum_{\substack{k=1 \\ \Omega_k^s \in \mathcal{T}_h^*}}^{N_s} meas(\Omega_k^s) [\sigma - \bar{\sigma}^{(k)}(u_h)]^T D^{-1} [\sigma - \bar{\sigma}^{(k)}(u_h)] \right\}^{1/2}, \quad (63)$$

where  $\sigma$  is the analytical solution for the stresses and  $\bar{\sigma}^{(k)}(u_h) = D\bar{\varepsilon}^{(k)}(u_h)$  is derived from smoothed strain solutions  $\varepsilon^{(k)}$  on smoothing domains  $\Omega_k^s$ .

For the bES-FEM method, it is also based on  $N_s$  smoothing domain  $\Omega_k^s \in \mathcal{T}_h^*$ , but the definition of its energy error norm depends on the displacement and pressure

$$\|u - u_h\|_E = \left\{ \begin{aligned} & 2\mu \sum_{\substack{k=1 \\ \Omega_k^s \in \mathcal{T}_h^*}}^{N_s} meas(\Omega_k^s) [\varepsilon(u) - \bar{\varepsilon}^{(k)}(u_h)]^T D_\mu [\varepsilon(u) - \bar{\varepsilon}^{(k)}(u_h)] \\ & + \sum_{\substack{k=1 \\ \Omega_k^s \in \mathcal{T}_h^*}}^{N_s} \int_{\Omega_k^s} [p(x) - p_h] [\nabla \cdot u(x) - (\overline{\nabla \cdot u_h})|_{\Omega_k^s}] dx \end{aligned} \right\}^{1/2}. \quad (64)$$

For the MINI method, its energy error norm which is evaluated on  $N_e$  triangles  $T_e \in \mathcal{T}_h$  is written as

$$\|u - u_h\|_E = \left\{ \begin{aligned} & 2\mu \sum_{\substack{e=1 \\ T_e \in \mathcal{T}_h}}^{N_e} meas(\Omega_k^s) [\varepsilon(u) - \varepsilon(u_h)]^T D_\mu [\varepsilon(u) - \varepsilon(u_h)] \\ & + \sum_{\substack{e=1 \\ T_e \in \mathcal{T}_h}}^{N_e} \int_{T_e} [p(x) - p_h] [\nabla \cdot u(x) - \nabla \cdot u_h] dx \end{aligned} \right\}^{1/2}. \quad (65)$$

## 6 Numerical results

In this section, we show some numerical results to estimate the efficiency and accuracy of the bES-FEM method. For this objective, we use the following benchmark problems to compare between the bES-FEM method and the above methods:

The first benchmark problem is considered to be the Cook's membrane problem. This well-known problem is often used to test for bending behavior and volumetric locking [46], [26], [40], [13]. Let  $\Omega$  is the convex hull

$$\Omega = conv\{(0, 0), (48, 44), (48, 60), (0, 44)\}.$$

The domain  $\Omega$  is the tapered panel (see Figure 9) whose left boundary is clamped, and whose right one is subjected to an in-plane shearing load of  $1N$  along the  $y$ -direction. The two material coefficients are the Young modulus  $E = 1$  and the Poisson ratio  $\nu = 0.4999999$ , which follows the nearly incompressible case. For this problem, the vertical displacement at the center tip section is found to be 18.5002 [38].

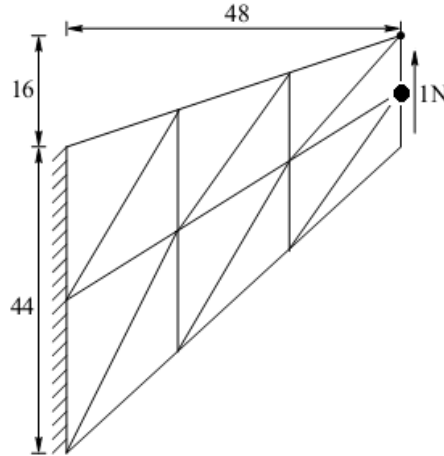


Figure 9. Cook's membrane problem on the primal triangulation.

In Figures 10, 11 and 12, we represent the comparison of numerical results between the bES-FEM and other methods for the Cook's membrane problem.

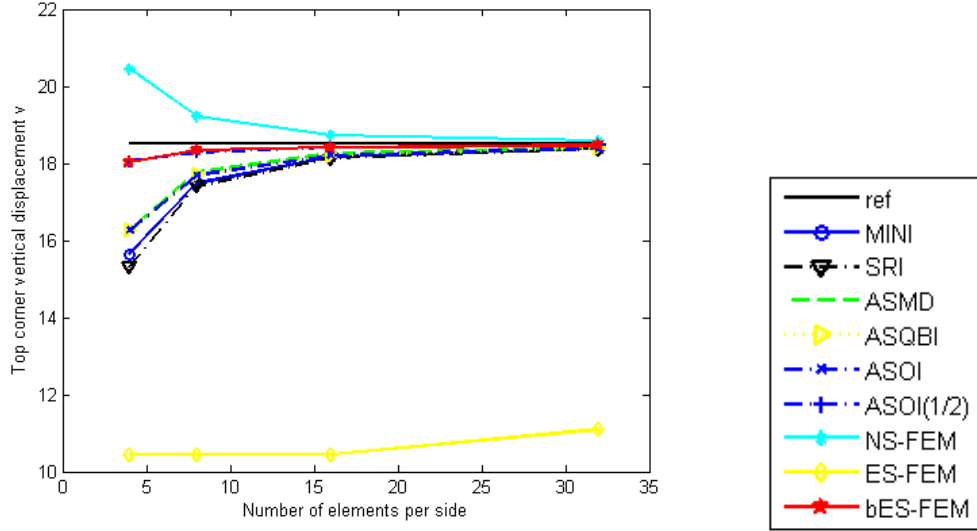
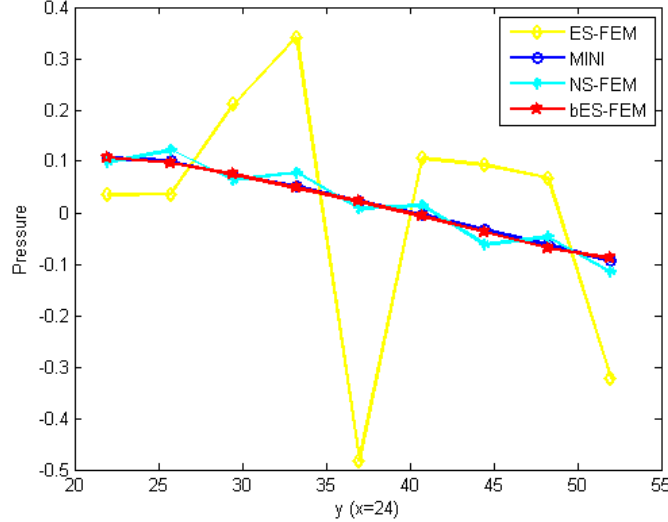


Figure 10. Convergence of displacement tip for Cook's membrane problem ( $\nu = 0.4999999$ ), where the reference solution is denoted by ref (the solid black line).

As shown in Figure 10, it is evident that the bES-FEM method is the most accurate than the other methods. Moreover, both ES-FEM and Q4 methods are subjected to volumetric locking. The NS-FEM method gives an upper bound solution and procedures quite well displacement tip without oscillations. Unfortunately, this method can no longer be guaranteed the stability of the pressure (see Figure 11).

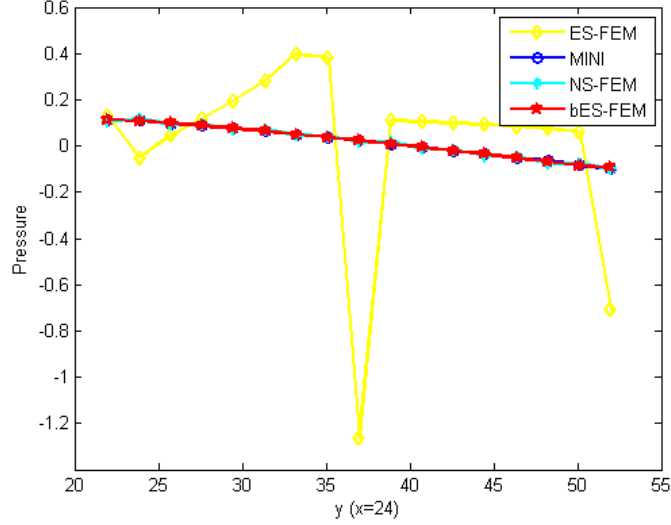


Mesh  $8 \times 8$

Figure 11. Pressure along the line  $y$  ( $x = 24$ ) for Cook's membrane problem ( $\nu = 0.4999999$ ).

Figure 11 illustrates the pressure distributions whose both the MINI element and the bES-FEM method are stable, and whose the NS-FEM method exhibits oscillations. However, for instability of the NS-FEM method, it is worth to note that this

problem is significantly improved (see Figure 12), when we use the finer triangular mesh  $16 \times 16$ . Besides, the two figures 11 and 12 indicate that the pressure results of both the ES-FEM method is very unstable.



Mesh  $16 \times 16$

Figure 12. Pressure along the line  $y$  ( $x = 24$ ) for Cook's membrane problem ( $\nu = 0.4999999$ ).

The next benchmark problem, considered in [10] and [46], is a cylindrical pipe subjected to an inner pressure  $p = 8kN/m^2$ , where its internal radius and external radius are  $a = 1m$   $b = 2m$ , respectively (see Figure 13).

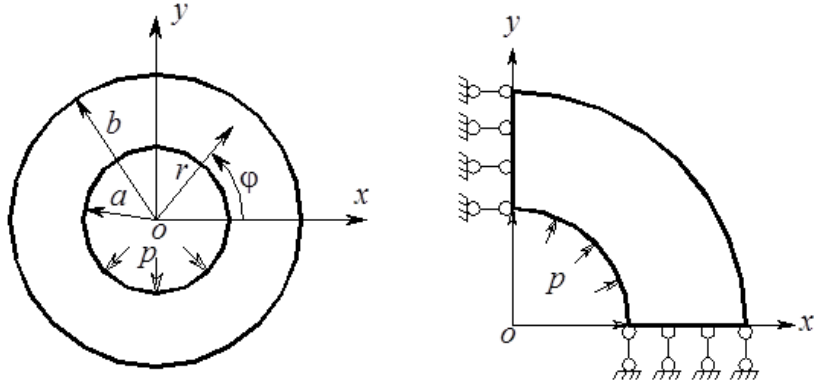
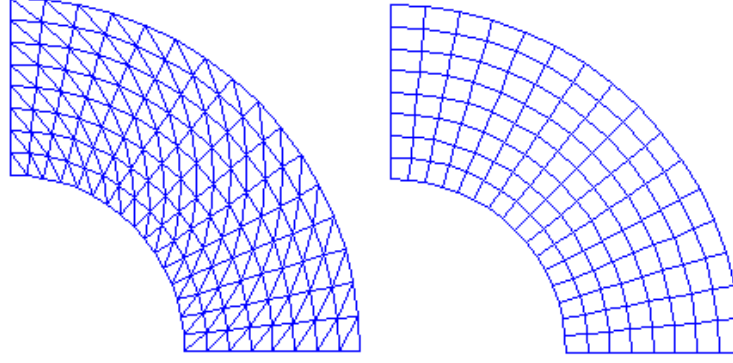


Figure 13. A cylindrical pipe subjected to an inner pressure and its quarter model with symmetric conditions imposed on the left and bottom edges.

Due to the axisymmetric characteristic of the problem, we model the upper right quadrant of the pipe imposed symmetric conditions on the left, bottom edges, and a free traction on its outer boundary. This problem is interested in the nearly incompressible case, *i.e* the Poisson ratio  $\nu$  is close to 0.5, to evaluate frame invariance and plane bending. Its domain is meshed by 3-node triangular and 4-node quadrilateral elements as shown in Figure 14.





a) 16x8x2 triangular elements b) 16x8 quadrilateral elements

Figure 14. a) domain discretization of 3-node triangular b) 4-node quadrilateral elements.

Additionally, the cylindrical pipe problem, which satisfies plane strain conditions and Young's modulus  $E = 21000kN/m$ , has its exact solution for the radial and tangential exact displacement [53]

$$u_r(r) = \frac{(1 + \nu)a^2p}{E(b^2 - a^2)} \left[ (1 - 2\nu) + \frac{b^2}{r} \right] \quad \text{and} \quad u_\varphi = 0 \quad (66)$$

and for the radial and tangential exact stresses

$$\sigma_r(r) = \frac{a^2p}{b^2 - a^2} \left( 1 - \frac{b^2}{r^2} \right), \quad \sigma_\phi(r) = \frac{a^2p}{b^2 - a^2} \left( 1 + \frac{b^2}{r^2} \right), \quad \sigma_{r\varphi} = 0. \quad (67)$$

In two equations (66) and (67),  $(r, \varphi)$  are the polar coordinates, and  $\varphi$  is measured counter-clockwise from the positive x-axis.

The MINI, NS-FEM, bES-FEM methods are used to investigate the convergence rate of this problem with the Poisson ratio  $\nu = 0.4999999$  whose results illustrate in Figure 15, 16 and 17

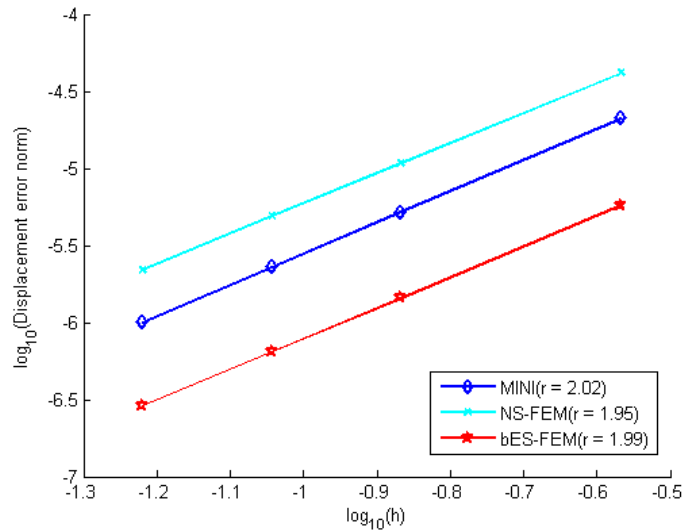


Figure 15. Displacement error norms of the bES-FEM method in comparison with the NS-FEM and MINI method for the cylindrical pipe under nearly incompressible condition ( $\nu = 0.4999999$ ).

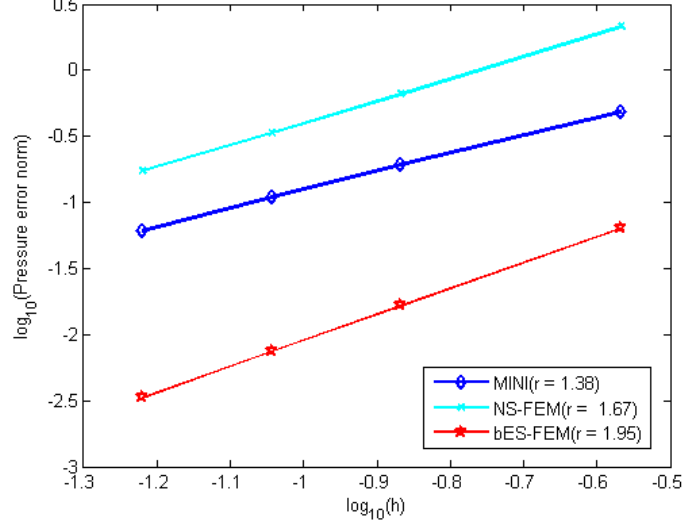


Figure 16. Pressure error norms of the bES-FEM method in comparison with the NS-FEM and MINI method for the cylindrical pipe under nearly incompressible condition ( $\nu = 0.4999999$ ).

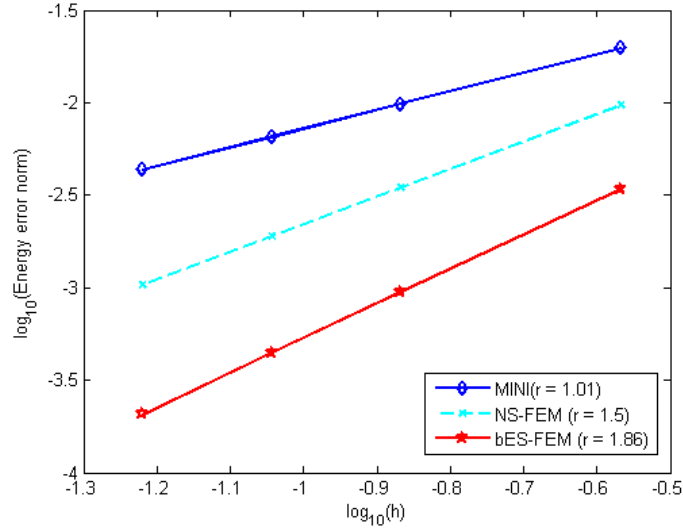


Figure 17. Energy error norms of the bES-FEM method in comparison with the NS-FEM and MINI method for the cylindrical pipe under nearly incompressible condition ( $\nu = 0.4999999$ ).

According to Figures 15 and 16, the two convergence rates in both the displacement and the pressure error norms of the bES-FEM method are very high ( $\geq 1.95$ ). With the MINI and NS-FEM methods, their convergence rates in the displacement error norm are close to 2, but their convergence rates in the pressure error norm are not as high as that of the bES-FEM method. Moreover, both the displacement and the pressure error norms of the bES-FEM method are more accuracy than ones of the MINI and NS-FEM methods. Besides, Figure 17 indicates that the error in energy norm for the bES-FEM method is smaller than those of the MINI and NS-FEM methods.

## 7 Conclusion

In this work, we have presented an edge-based smoothed element method enriched with bubble functions (bES-FEM) for nearly incompressible 2D-3D elasticity. The method help soften the bilinear form allowing the weakened weak (W2) procedure to get a quality solution. For the bES-FEM method, we show that the uniform inf-suf condition satisfies. Besides, the degree of freedom for the pressure can be computed by linear combinations depending on the displacement, then the mixed displacement-pressure formulation is based only on displacements.

## References

- [1] D. Arnold and R. Winther. *Mixed finite elements for elasticity*. Numerische Mathematik, 92, 401-419, (2002).
- [2] D. Arnold, F. Brezzi, M. Fortin. *A stable finite element for the Stokes equations*. Calcolo, 21: 337-344, (1984).
- [3] I. Babuška and M. Suri Locking effects in the Finite Element approximation of Elasticity problems. Numerische Mathematik , 62, 439-463, (1992).
- [4] I. Babuška and M. Suri. On locking and robustness in the finite element method. SIAM Journal on Numerical Analysis, 29, 1261-1293, (1992).
- [5] F. Brezzi and M. Fortin. *Mixed and hybrid finite element methods*. SpringerVerlag, New York, (1991) .
- [6] F. Brezzi and J. Pitk'aranta. *On the stabilization of finite element approximations of the Stokes equation*. Wolfgang Hackbusch (Ed.), Efficient solution of elliptic systems proceeding of a GAMM-Seminar Kiel, January 27-28, 1984.
- [7] D. Braess. *Stability of saddle point problems with penalty*. Mathematical Modelling and Numerical Analysis, 30, 731-742, (1996) .
- [8] D. Braess. *Finite Elements. Theory, fast solver, and applications in solid mechanics*. Cambridge University Press, Second Edition, (2001).
- [9] F. Cazes and G. Meschke. *An edge-based smoothed finite element method for 3D analysis of solid mechanics problems*. Int. J. Numer. Meth. Engng, Published online in Wiley Online Library (wileyonlinelibrary.com). DOI: 10.1002/nme.4472, (2013).
- [10] T. Belytschko, E. Bachrach. *Efficient implementation of quadrilaterals with high coarse-mesh accuracy*. Computer Methods in Applied Mechanics and Engineering, 54:279-301, (1986).
- [11] T. Belytschko, W. K. Liu and B. Moran. *Nonlinear finite elements for continua and structures*. John Wiley & Sons, Ltd, (2001).
- [12] J. S. Chen, C. T. Wu, S. Yoon, Y. You. *A stabilized conforming nodal integration for Galerkin mesh-free methods*. International Journal for Numerical Methods in Engineering, 50:435-466, (2001).
- [13] R. Cook. *Improved twodimensional finite element*. Journal of the Structural Division, (ASCE); 100: 1851 - 1863, (1974).

- [14] D. P. Flanagan and T. A. Belytschko. *A uniform strain hexahedron and quadrilateral with orthogonal hourglass control*. International Journal for Numerical Methods in Engineering, 17:679706, (1981).
- [15] T. Hughes. *The finite element method: Linear, static and dynamic finite element analysis*, Prentice-Hall, (1987).
- [16] D. Kosloff, G. A. Frazier. *Treatment of hourglass patterns in low order finite element codes*. International Journal for Numerical and Analytical Methods in Geomechanics, 2:5772, (1978).
- [17] G. R. Liu. *A  $G$  space theory and a weakened weak ( $W^2$ ) form for a unified formulation of compatible and incompatible methods: Part I theory*. Int. J. Numer. Meth. Engng, 81: 1093-1126, (2010).
- [18] G. R. Liu. *A  $G$  space theory and a weakened weak ( $W^2$ ) form for a unified formulation of compatible and incompatible methods: Part II applications to solid mechanics problems*. Int. J. Numer. Meth. Engng, 81: 1127-1156, (2010).
- [19] G. R. Liu. *Mesh-free methods: moving beyond the finite element method*. CRC Press, Boca Raton, 2nd Edition, (2009).
- [20] G.R. Liu and T. Nguyen-Thoi. *Smoothed Finite Element Methods*, CRC Press, Taylor and Francis Group, New York, (2010).
- [21] G. R. Liu, Dai KY, Nguyen-Thoi T. *A smoothed finite element for mechanics problems*. Computational Mechanics, 39:859877, (2007).
- [22] G. R. Liu GR, Nguyen-Thoi T, Nguyen-Xuan H, Lam KY. *A node based smoothed finite element method (NS-FEM) for upper bound solution to solid mechanics problems*. Computers and Structures, 87:14-26, (2009).
- [23] G. R. Liu, Nguyen-Thoi T, Lam KY. *An edge-based smoothed finite element method (ES-FEM) for static, free and forced vibration analyses of solids*. Journal of Sound and Vibration, 320: 1100-1130, (2009).
- [24] Nguyen-Thoi T, G. R Liu, Lam KY, Zhang GY. *A Face-based Smoothed Finite Element Method (FS-FEM) for 3D linear and nonlinear solid mechanics problems using 4-node tetrahedral elements*. International Journal for Numerical Methods in Engineering, 78: 324-353, (2009).
- [25] J. Matsumoto. *A relationship between stabilization FEM and Bubble function element stabilization method with orthogonal basis for incompressible flows*. Journal of Applied Mechanics Vol. 8 (2005).
- [26] B. Lamichhane. *Inf-sup stable finite-element pairs based on dual meshes and bases for nearly incompressible elasticity*. IMA Journal on Numerical Analysis, volume 29, page 404-420, (2009).
- [27] Robert A. Adams, John J. F. Fournier. *A Sobolev space*, Elsevier, Volume 140, Second Edition (Pure and Applied Mathematics), (2003).
- [28] R. Pierre, *Regularization procedures of mixed finite element approximations of the Stokes problem*. Rapports de Recherche, INRIA, N° 673, (1987).
- [29] O. C. Zienkiewicz and R. L. Taylor, *The Finite Element Method, fifth ed. (vol.1)*. Butterworth Heinemann, Oxford, (2000).

- [30] Dai KY and G. R. Liu. *Free and forced vibration analysis using the smoothed finite element method (SFEM)*. Journal of Sound and Vibration, 301:803820, (2007).
- [31] Nguyen-Xuan H, T. Rabczuk, S. Bordas, J. F. Debongnie. *A smoothed finite element method for plate analysis*. Computer Methods in Applied Mechanics and Engineering, 197: 1184-1203, (2008).
- [32] Nguyen-Xuan H, Nguyen-Thoi T. *A stabilized smoothed finite element method for free vibration analysis of Mindlin-Reissner plates*. Communications in Numerical Method and Engineering, 25 (8): 882 - 906, (2009).
- [33] Nguyen-Thanh N, T. Rabczuk, Nguyen-Xuan H, S. Bordas. *A smoothed finite element method for shell analysis*. Computer Methods in Applied Mechanics and Engineering, 198: 165-177, (2008).
- [34] Nguyen-Xuan H, G. R. Liu, Nguyen-Thoi T, Nguyen-Tran C. *An edge-based smoothed finite element method (ES-FEM) for static, free and forced vibration analyses of solids*. Smart Material and Structures, 18: 065015, (2009)
- [35] Tran TN, G. R. Liu, Nguyen-Xuan H, Nguyen-Thoi T. *An edge-based smoothed finite element method for primal-dual shakedown analysis of structures*. International Journal of Numerical Methods in Engineering, 82: 917-938, (2010).
- [36] Le CV, Nguyen-Xuan H, Askes H, Bordas S, Rabczuk T, Nguyen-Vinh H. *A cell-based smoothed finite element method for kinematic limit analysis*. International Journal of Numerical Methods in Engineering 2010; 83:16511674.
- [37] G. R. Liu, N. Nourbakhshnia, Y. W. Zhang. *A novel singular ES-FEM method for simulating singular stress fields near the crack tips for linear fracture problems*. Engineering Fracture Mechanics, 78: 863876, (2011).
- [38] G. R. Liu, Nguyen-Xuan H, Nguyen-Thoi T. *A variationally consistent aFEM (VCaFEM) for solution bounds and nearly exact solution to mechanics problems using quadrilateral elements*. International Journal for Numerical Methods in Engineering, 85 (4): 403536, (2011).
- [39] R. Piltner R, R. L. Taylor. *Triangular finite elements with rotational degrees of freedom and enhanced strain modes*. Computers and Structures; 75: 361-368, (2000).
- [40] J. C. Simo, M. S. Rifai. *A class of mixed assumed strain methods and the method of incompatible modes*. International Journal for Numerical Methods in Engineering, 29: 1595 1638, (1990).
- [41] R. P. R Cardoso, J. W. Yoon, Mahardika, S. Choudhry, R. J. Alves de Sousa, R. A. Fontes Valente. *Enhanced assumed strain (EAS) and assumed natural strain (ANS) methods for one-point quadrature solid-shell elements*. International Journal for Numerical Methods in Engineering, 75: 156 187, (2008).
- [42] D. Kosloff D, G. A. Frazier. *Treatment of hourglass patterns in low order finite element codes*. International Journal for Numerical and Analytical Methods in Geomechanics, 2: 57 72, (1978).

- [43] D. P. Flanagan, T. Belytschko. *A uniform strain hexahedron and quadrilateral with orthogonal hourglass control*. International Journal for Numerical Methods in Engineering, 17: 679–706, (1978).
- [44] T. Belytschko, W. E. Bachrach. *Efficient implementation of quadrilaterals with high coarse-mesh accuracy*. Computer Methods in Applied Mechanics and Engineering, 54: 279–301, (1986).
- [45] T. Belytschko, L. P. Bindeman. *Assumed strain stabilization of the 4-node quadrilateral with 1-point quadrature for nonlinear problems*. Computer Methods in Applied Mechanics and Engineering 1993; 88: 311–340.
- [46] M. Fredriksson, N. S. Ottosen. *Fast and accurate 4-node quadrilateral*. International Journal for Numerical Methods in Engineering, 61: 1809–1834, (2004)
- [47] T. H. H. Pian, C. C. Wu. *Hybrid and Incompatible Finite Element Methods*. CRC Press: Boca Raton, FL, 2006.
- [48] J. Bonet, A. J. Burton. *A simple average nodal pressure tetrahedral element for incompressible and nearly incompressible dynamic explicit applications*. Communications in Numerical Methods in Engineering, 14: 43744, (1998).
- [49] J. Bonet, H. Marriott, O. Hassan. *Stability and comparison of different linear tetrahedral formulations for nearly incompressible explicit dynamic applications*. International Journal for Numerical Methods in Engineering, 50, 119133, (2001).
- [50] E. A. De Souza Neto, F. M. A. Pires, D. R. J. Owen. *F-bar-based linear triangles and tetrahedra for finite strain analysis of nearly incompressible solids. part I: formulation and benchmarking*, International Journal for Numerical Methods in Engineering, 62, 353383, (2005).
- [51] F. M. A. Pires, E. A. De Souza Neto, J. L. De La Cuesta Padilla. *An assessment of the average nodal volume formulation for the analysis of nearly incompressible solids under finite strains*. Communications in Numerical Methods in Engineering, 20, 569583, (2004).
- [52] R. L. Taylor, P. J. Beresford and E. L. Wilson. *A non-conforming element for stress analysis*. International Journal for Numerical Methods in Engineering, 10: 12111219, (1976).
- [53] S. P. Timoshenko, J. N. Goodier. *Theory of Elasticity (3rd edn)*. McGraw-Hill, NewYork, 1970.